Modelling of plasma-based dry reforming : how do uncertainties in the input data affect the calculation results?

Modelling of plasma-based dry reforming: How do uncertainties in the input data affect the calculation results?

Weizong Wang*, Antonin Berthelot, Quanzhi Zhang, and Annemie Bogaerts*

Research group PLASMANT, Department of Chemistry, University of Antwerp, Universiteitsplein 1, B-2610 Wilrijk-Antwerp, Belgium

*E-mail: wangweizong@gmail.com, annemie.bogaerts@uantwerpen.be

* Author to whom any correspondence should be addressed.

Abstract

One of the main issues in plasma chemistry modeling is that the cross sections and rate coefficients are subject to uncertainties, which yields uncertainties in the modeling results and hence hinders the predictive capabilities. In this paper we reveal the impact of these uncertainties on the model predictions of plasma-based dry reforming in a dielectric barrier discharge. For this purpose, we performed a detailed uncertainty analysis and sensitivity study. 2000 different combinations of rate coefficients, based on the uncertainty from a log-normal distribution, are used to predict the uncertainties in the model output. The uncertainties in the electron density and electron temperature are around 11% and 8% at the maximum of the power deposition for a 70% confidence level. Still, this can have a major effect on the electron impact rates and hence on the calculated conversions of CO_2 and CH_4, as well as on the selectivities of CO and H_2. For the CO_2 and CH_4 conversion, we obtain uncertainties of 24% and 33%, respectively. For the CO and H_2 selectivity, the corresponding uncertainties are 28% and 14%, respectively. We also identify which reactions contribute most to the uncertainty in the model predictions. In order to improve the accuracy and reliability of plasma chemistry models, we recommend using only verified rate coefficients, and we point out the need for dedicated verification experiments.

Keywords

Plasma chemistry modelling, rate coefficients, uncertainties, DBD plasma, dry reforming, CO_2 and CH_4 conversion, selectivities

1. Introduction

In recent decades, there is growing concern on global climate change caused by the increased accumulations of anthropogenic greenhouse gases. The conversion of the main greenhouse gases (CO_2 and CH_4) to value-added chemicals or renewable fuels is an effective strategy to reduce these accumulations. This conversion is considered one of the challenges of the 21st century [1]-[2]. It fits into the visionary "cradle-to-cradle" concept, converting waste (greenhouse gases) into a new feedstock (fuels and raw materials) [3].

The combined conversion of both CH_4 and CO_2, i.e. dry reforming of methane (DRM, see reaction (1)), has indeed gained significant interest over the years, as it can realize greenhouse gas reduction and utilization by the formation of syngas (H_2+CO), a versatile product that can serve not only as fuel, but also as feedstock for value-added chemicals and liquid fuels. Indeed, syngas can be utilized in a variety of downstream processes, such as methanol (CH_3OH) synthesis, Fischer-Tropsch (F-T) synthesis, and several other carboxylation and hydrogenation processes [4]-[6]. The main advantage of DRM over other reforming processes is that CO_2 is used as both a carbon source and oxidizing agent and it produces syngas in a ratio which is easily controllable. However, the conventional catalytic DRM process suffers from severe drawbacks that hamper its industrial application, e.g., the high energy cost at high temperature (≥ 700℃), rapid deactivation of the catalyst caused by the inevitable carbon deposition leading to catalyst poisoning or active metal sintering, and a slow start-up time [7]-[8].

$$CH_4 + CO_2 \rightarrow 2CO + 2H_2 \quad \Delta H^o = 247 \text{ kJ/mol} \tag{1}$$

These challenges have led to a major interest in alternative reforming techniques in pursuit of milder reaction conditions with reduced energy costs. In this respect, atmospheric non-equilibrium plasmas offer unique perspectives, because of their capacity to induce chemical reactions within gases with a limited energy cost at mild conditions, as well as their easy operation, quick and efficient reaction process [9]. Indeed, non-equilibrium cold plasmas exhibit a much higher electron temperature than gas temperature, and the highly energetic electrons can activate the stable molecules (e.g., CO_2 and CH_4) and initiate reactions by electron impact collisions rather than by gas heating, enabling endothermic reactions to occur at relatively low gas temperature. A lot of research is being performed to improve the process, and depending on the type of plasma source, it might be competitive already with other emerging technologies [9]. We believe that plasma might be quite promising for this application, when it is generated from renewable energy sources (wind or solar), as it can be switched on/off very quickly, so it might be suitable for storage of peak powers in renewable electricity. One example of such a non-thermal plasma is a dielectric barrier discharge (DBD), which is created by applying a potential difference between two electrodes, of which at least one is covered by a dielectric layer. A DBD reactor has a very simple design, which is beneficial for later up-scaling to real applications, as was demonstrated already 100 years ago for commercial ozone synthesis [10]. Many experiments have already been performed for DRM in a DBD reactor [11]-[30].

Besides experiments, detailed modelling is very useful to obtain a better insight in the underlying plasma processes and to improve the applications [31]-[33]. A variety of models have been developed in literature for DRM [34]-[39]. In particular, a plasma chemical kinetics model is an effective tool to provide a deeper understanding of the underlying chemical reactions occurring in the plasma for which direct measurements are not always straightforward [34].

One of the main issues encountered when developing such a chemical kinetics model is that the rate coefficients and cross sections used are subject to uncertainties, causing also uncertainties in the modeling results, which hinders the predictive capabilities [40]. A detailed uncertainty analysis and

sensitivity study is therefore needed to reveal the impact of these uncertainties on the model predictions. Such an analysis was presented already by Turner for a He/O_2 mixture, [41]-[43] and for a CO_2 plasma in our group [44]. The current paper continues along these lines and extends the analysis to the plasma chemistry modelling of DRM in a DBD reactor.

2. Description of the model

We first describe the zero-dimensional (0D) chemical kinetics model (section 2.1), followed by the chemistry set for DRM in a DBD plasma (section 2.2). Finally, we explain the procedure to determine the uncertainty in the output and we describe the statistical treatment to deal with the data (section 2.3).

2.1 Zero-dimensional (0D) chemical kinetics model and its application to a DBD reactor

We use a 0D chemical kinetics model, implemented in the ZDPlaskin code [45], to elucidate the plasma chemistry. This model calculates the species densities as a function of time by means of continuity equations, taking into account the various production and loss terms:

$$\frac{dn_i}{dt} = \sum_j \left\{ \left(a_{ij}^{(2)} - a_{ij}^{(1)} \right) k_j \prod_l n_l^{a_{lj}^{(1)}} \right\} \quad (2)$$

where $a_{ij}^{(1)}$ and $a_{ij}^{(2)}$ are the stoichiometric coefficients of species i, at the left and right hand side of a reaction j, respectively, n_l is the species density at the left-hand side of the reaction, and k_j is the rate coefficient of reaction j (see below).

In a 0D model, transport processes are neglected; hence, the species densities are assumed to be constant in the entire simulation volume. However, we can translate the temporal behavior into a spatial behavior (i.e., as a function of distance along the DBD tube) by means of the gas velocity, determined by the mass flow rate (i.e., similarity between batch reactor and plug flow reactor). This allows us to mimic the typical filamentary behavior of a DBD used for gas conversion. Indeed, the gas molecules will pass through several microdischarge filaments on their way throughout the reactor. This is taken into account in the model by applying a large number of consecutive microdischarge pulses and their afterglows as a function of time. We assume a triangular pulse of power deposition, with a duration of 60 ns for each pulse, and an interpulse time of 0.29 s. In this way, we describe 47 pulses over a gas residence time of 13.7 s. The gas temperature remains close to room temperature under these experimental conditions [13], so we can ignore the effect of gas heating during the conversion and use a constant gas temperature of 300 K in the simulation. The same parameters have also been applied for describing the microdischarge behavior for pure CO_2 in our group [46]. The maximum power of the pulses is chosen in such a manner that the specific energy input (SEI), determined by total power deposition and gas flow rate (or residence time), can be compared with experimental results for validation (see below). This approach was proven to be successful for a variety of conditions and gas mixtures [34].

The calculated conversions of CO_2 and CH_4 are defined as:

$$X_{CO2} = \frac{\text{Moles of } CO_2 \text{converted}}{\text{Moles of } CO_2 \text{ input}} \times 100\% \quad (3)$$

$$X_{CH_4} = \frac{\text{Moles of } CH_4 \text{converted}}{\text{Moles of } CH_4 \text{ input}} \times 100\% \quad (4)$$

The selectivity of H_2 and CO is defined as follows:

$$S_{H2} = \frac{\text{Moles of } H_2 \text{produced}}{2 \times \text{Moles of } CH_4 \text{ converted} + \text{Moles of } H_2O \text{ converted}} \times 100\% \quad (5)$$

$$S_{\mathrm{CO}} = \frac{\text{Moles of CO produced}}{\text{Moles of } CH_4 \text{ converted} + \text{Moles of } CO_2 \text{ converted}} \times 100\% \quad (6)$$

2.2 Plasma chemistry set

We recently developed an extensive plasma chemistry model for DRM in a DBD, validated by experiments [34]. However, the number of species and chemical reactions included in this model is very large. Such a complicated plasma chemistry set makes detailed uncertainty analysis and sensitivity studies computationally expensive, and also quite challenging, because of the need to trace back the corresponding uncertainties for all input data. Therefore, we reduced this chemistry set, by removing all species that do not significantly contribute to the plasma chemistry. The species considered in this reduced model are listed in table 1. The model considers 71 different species, including the electrons, various molecules, radicals, ions and excited species. Two electronically excited levels for CO_2, with threshold energies at 7.0 eV and 10.5 eV, are included in the model, i.e., CO_2 (e1) and CO_2 (e2), as well as the first vibrationally excited state of H_2 and the lowest electronically excited state $H_2(B^3\Sigma)$, i.e., indicated in table 1 as H_2 (v) and H_2 (e). Although electron impact vibrational excitation is included in the calculation of the electron energy distribution function (EEDF), the model does not include the vibrationally excited states of CO_2 and CH_4 because they are of minor importance in DBD plasma conditions [50].

These 71 species react with each other through 114 electron impact reactions, 43 ion-neutral and ion-ion reactions, and 128 neutral reactions. These reactions are listed in the Appendix. These reactions are listed in the Appendix. Note that tables A.1 and A.2 only list 55 and 33 electron reactions. The remaining reactions are electron impact reactions (ionization, attachment dissociation etc.) from the excited species, as well as the superelastic reactions, i.e. the reverse processes of electron impact excitation.

The rate coefficients for the electron impact reactions are a function of the average electron energy and calculated based on the electron energy distribution function (EEDF) with a Boltzmann solver, BOLSIG$^+$, [47] which is integrated into ZDPlaskin. The EEDF is calculated with the same set of cross sections as used for the chemical kinetics part (table A1 in the Appendix), including superelastic collisions. Table A2 presents the electron impact reactions described by analytic expressions for the rate coefficients. The rate coefficients of the heavy particle reactions (i.e., atoms, molecules, radicals, ions and excited species) depend on the gas temperature and are adopted from literature. Table A3 shows the ion-neutral and ion-ion reactions and table A4 presents the reactions between the neutral species. The references where these data are adopted from, as well as the corresponding uncertainties reported for these values, are also included in these tables. The latter are needed for the uncertainty and sensitivity analysis, described in next section.

Table 1 Overview of the species included in the model

Molecules	Charged species	Radicals	Excited species
CH_4 , C_2H_2, C_2H_4, C_2H_6,C_3H_6, C_3H_8	CH_5^+, CH_4^+, CH_3^+,$C_2H_6^+$, $C_2H_5^+$,$C_2H_4^+$, $C_2H_3^+$, $C_2H_2^+$	CH_3, CH_2, CH, C, C_2H_5, C_2H_3, C_2H, C_3H_7	
CO_2, CO	CO_2^+, CO^+,CO_3^-, CO_4^-, $C_2O_4^+$, $C_2O_3^+$, $C_2O_2^+$		CO_2(e1), CO_2(e2)
H_2O	H_3O^+, OH^-	OH, HO_2	
CH_3OH, CH_3CHO, C_2H_5OH, C_2H_5OOH, CH_2CO, CH_2O		CHO, CH_2OH, CH_3O, C_2HO, CH_3CO, CH_2CHO, C_2H_5O, $C_2H_5O_2$	

H_2	H_2^+, H^+, H^-	H	$H(2P), H_2(v), H_2(e)$
O_3, O_2	O_3^-, O_2^-, O^-	O	$O(1D), O(1S), O_2(a1), O_2(b1)$
	e^-		

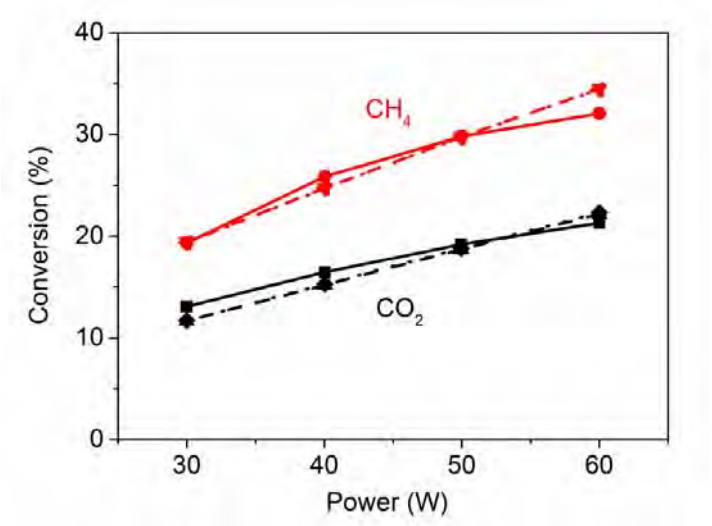

Figure 1 CO_2 and CH_4 conversion, calculated with the full (dashed lines) and reduced (dotted lines) plasma chemistry set, in comparison to the measured data (solid lines; adopted from ref. [13] and [36]) in a 1:1 CO_2/CH_4 mixture at a total flow rate of 50 sccm, as a function of discharge power. The calculation results with full and reduced chemistry set overlap, indicating that the reduced set captures the most important chemistry.

Figure 1 illustrates the calculated CH_4 and CO_2 conversions as a function of discharge power, obtained by the full and the reduced chemistry set, in comparison with experimental values obtained from ref. [13] and [36], for a DBD in a 1:1 CO_2/CH_4 mixture at a total flow rate of 50 sccm. Very good agreement is reached between the calculated and experimental conversions, both for the full and reduced chemistry set, showing that our chemical kinetics model, with both chemistry sets, can provide a realistic picture of the plasma chemistry of DRM in the DBD reactor.

2.3 Uncertainty analysis and computational procedure

The experimentally derived rate coefficients for the heavy particle reactions are either constant or follow an Arrhenius expression (7); see Tables A.3-A.4 in the Appendix.

$$k = AT_g^B exp(-\frac{E_a}{k_B T_g}) \quad (7)$$

where k is the rate coefficient, k_B is the Boltzmann constant, T_g the gas temperature and E_a the activation energy. The parameters A and B are experimentally or theoretically determined. For the chemical reactions involving electrons, the rate constants are either obtained from the energy-dependent cross sections (Table A.1), or they are constant or show a dependence on the electron temperature T_e (Table A.2). Each of the parameters in the expressions for the rate coefficients (i.e., E_a, A and B in the Arrhenius expression, or the parameters for the T_e dependence) may bring some uncertainties. However, following the approach of Turner [41]-[43], we only consider the uncertainty of the parameter A. The motivation is that for the rate coefficients derived from the energy-dependent

cross sections, we can assume that the shape of the cross sections is better known than the absolute value, as is indeed often the case for data originating from beam measurements. Additionally, the uncertainty for parameters B and E_a is rarely presented when the rate coefficient is reported in the form of equation (7). The assumption that only A is uncertain is therefore not only convenient, but it also reflects the character of the data practically available. Indeed, as long as the rate coefficient is used in the parameter range considered for determining the analytical expression, i.e. $\frac{\Delta k}{\bar{k}} = \frac{\Delta A}{\bar{A}}$, where ΔX refers to the uncertainty on a quantity X and $\bar{X}$ refers to its mean value, the uncertainty in the rate coefficient can be considered to be included in the pre-exponential factor A. In the same way, the uncertainty in the cross sections can also be described by the uncertainty in the absolute value of these cross sections.

We characterize the uncertainty in each rate coefficient by a log-normal distribution. This choice is debatable, as some of the extreme values for the rate coefficients may be non-physical [34]. Nevertheless, we believe it gives a good estimation of the uncertainties in the model, and as we focus on the different quantiles in the outcome of the simulations (see below), our approach avoids these non-physical values [44]. The probability $f\,(A_n = x_A;\, \Delta A, \bar{A}\,)$ that the coefficient A in equation (7) has a value x_A, given its uncertainty ΔA and mean value $\bar{A}$, is given by a log-normal distribution [48]:

$$f(A_n = xA;\ \Delta A, \bar{A}) = \frac{1}{xA\sigma\sqrt{2\pi}} exp(-\frac{\ln(x_A-\mu)^2}{2\sigma^2}) \qquad (8)$$

where μ and σ are parameters that contain the mean value of A ($\bar{A}$) and the uncertainty ΔA.

$$\mu = ln(\frac{\bar{A}^2}{\sqrt{\bar{A}^2+\Delta A^2}}) \qquad \sigma = \sqrt{ln(1+(\frac{\Delta A}{\bar{A}})^2)} \qquad (9)$$

To define the uncertainties in the calculation results, based on the uncertainties of all rate coefficients, we create a large number (N = 2000) of different combinations of these rate coefficients. Each rate coefficient k_i of a given combination i is randomly determined, based on the probability density described in equation (8). For rate coefficients k' that are derived from another rate coefficient k (scaling laws, i.e., for the superelastic processes such as X4 and X5), we multiply the scaled rate coefficient $\bar{k'}$ by a factor $\frac{k_i}{\bar{k}}$, i.e. $k'_i = \bar{k'}\frac{k_i}{\bar{k}}$, for each combination i. We run the model for each combination of rate coefficients (i.e. 2000 different inputs) and the different outcomes yield the estimated uncertainty in the calculation results.

Furthermore, we also perform a correlation analysis between the input values taken for the various rate coefficients and a certain calculation output, to indicate which reaction is important for this output. For this purpose, we use the Spearman's ρ rank correlation coefficient, to rank which input is mostly correlated with which output. Indeed, the Spearman's ρ rank correlation coefficient is a nonparametric measure of rank correlation (statistical dependence between the rankings of two variables) [48]. It assesses how well the relationship between two variables can be described using a monotonic function, by which the main sources of uncertainty on a given output are identified. The Spearman's correlation between two variables is high when observations have a similar rank between both variables (i.e. relative position label of the observations within the variable: 1st, 2nd, 3rd, etc.), and low when observations have a dissimilar rank between the two variables. In the limit, they are identical for a correlation of 1, or fully opposed for a correlation of −1. By doing so, we can reveal the impact of the uncertainties of the various input data on the model predictions and obtain information on the main source of uncertainty in the model predictions.

3. Results and discussion

3.1 Effect of the uncertainties on the calculation results

We first investigate the influence of the uncertainties in the cross sections and rate coefficients on the calculated plasma properties, namely the electron density and electron temperature (figure 2), the CO_2 and CH_4 conversion during the first pulse (figure 3), the overall CO_2 and CH_4 conversion for the entire gas residence time (figure 4), and the corresponding selectivity of CO and H_2 (figure 5). The calculations are performed for a 1:1 CO_2/CH_4 mixture at a total flow rate of 50 sccm and discharge power of 60 W, yielding a specific energy input of 18.4 eV/molecule, which corresponds well to the experimental conditions used for the validation [13]. We also performed calculations for a wider power range, and the results are similar to those presented below for 60 W.

We use different colours in figures 2-5 to represent different confidence intervals for the calculation results. The confidence intervals of 90%, 70%, 50% and 25% correspond to the intervals of [X5, X95], [X15, X85], [X25, X75], and [X37.5, X62.5], respectively. We also show the median value of the N = 2000 cases with a black curve. Additionally, in the legends we present the (relative) uncertainties, i.e. relative error of the calculation results, for each confidence interval, to quantify the dispersion of the data. This uncertainty is defined as $(X_U - X_L)/X50/2\times100\%$, where X_U and X_L stand for the upper and lower quantile of each confidence interval. Note that the distribution of the data within the interval $[X - \sigma_X, X + \sigma_X]$ in a normal distribution, where σ_X is the standard deviation, is 68%. Therefore, unless mentioned otherwise, we focus on a confidence interval of 70%, although it should be realized that the distribution of the data is not completely symmetrical in our case.

In addition, in table 2, we summarize the median values of the calculated quantities, with their corresponding absolute uncertainties according to the different confidence intervals of 90%, 70%, 50% and 25%. The absolute (and relative) uncertainty is not necessarily the same in the positive and negative direction, as can be deduced from figures 2-5, but the difference is at maximum 20%, so for simplicity we present the average of both in table 2, i.e. $(X_U - X_L)/2$, which gives a reasonable indication.

Table 2 Summary of the median values of the calculated quantities, with their corresponding absolute uncertainties, according to different confidence intervals of 90%, 70%, 50% and 25%.

Quantity	Median value	Absolute uncertainty at different confidence intervals of			
		90%	70%	50%	25%
N_e (at max of pulse) in 10^{15} cm^{-3}	1.20	±0.18	±0.11	±0.08	±0.04
T_e (at max of pulse) in eV	2.60	±0.12	±0.08	±0.05	±0.02
X_{CO2} (at end of first pulse) (%)	0.65	±0.32	±0.20	±0.13	±0.06
X_{CH4} (at end of first pulse) (%)	1.30	±0.53	±0.32	±0.20	±0.10
Overall X_{CO2} (%)	21	±8	±5	±3	±2
Overall X_{CH4} (%)	33	±16	±11	±7	±3
Overall S_{CO} (%)	57	±25	±16	±10	±5
Overall S_{H2} (%)	57	±14	±8	±5	±2

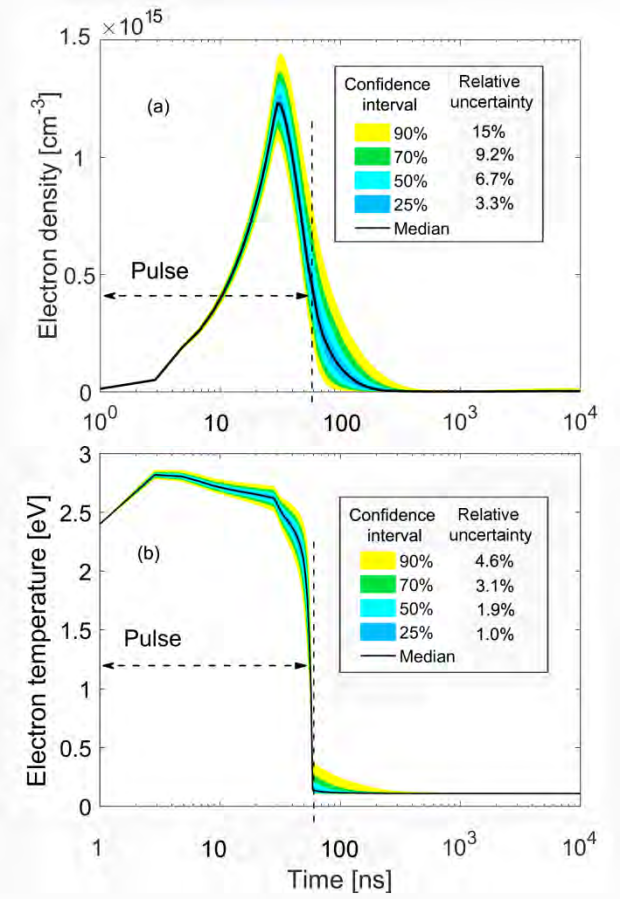

Figure 2 Electron density (a) and electron temperature (b) as a function of time for one microdischarge pulse and afterglow. The vertical dashed line at t = 60 ns indicates the end of the microdischarge pulse. The median value is shown by the black curve. The different colours delimit different quantiles of the N = 2000 calculation results at each time, as indicated by the legend, e.g, yellow means that 90% of the calculation results fall within that range, i.e., 90% confidence interval. The corresponding relative uncertainty (based on the relative difference between the upper and lower quantiles, divided by two) at the maximum of the power deposition is also indicated in the legends, for each confidence interval.

Figure 2 shows the electron density and electron temperature as a function of time for one microdischarge pulse and afterglow. The maximum power of the pulse was set to 4.25×10^7 W at 30 ns, to yield an overall power deposition of 60 W for the total residence time of 13.7 s, matching the conditions of a DBD with 47 consecutive microdischarge pulses. The calculated electron number density shows the same profile as the power deposition and decays exponentially at the end of each pulse. The electron temperature increases upon start of the discharge pulse, because the electrons are heated by the electric field. Upon termination of the pulse, the electron temperature drops to a background value of 0.10 eV, used to guarantee calculation convergence during the afterglow stage. The calculated median values show a maximum electron density of 1.20×10^{15} cm^{-3} and a maximum electron temperature of 2.6 eV. These values correspond well with experimental data in literature for microdischarge pulses [10], [49]. The relative uncertainties (defined as the relative difference between the upper quantile X_U and the lower quantile X_L divided by two) for electron density and electron temperature are 9.2% and 3.1 %, respectively, at the maximum of the power deposition, for a 70% confidence interval. The corresponding relative uncertainties for the other confidence intervals can be found in the legends, and the absolute uncertainties for both electron density and temperature are listed

in table 2. The fact that these relative (and absolute) uncertainties are relatively low may be explained by the fact that the uncertainties for the rate constants and cross sections of electron impact reactions are lower than those of the heavy particles reactions (see table A1-A4). However, the relative uncertainties for both electron density and temperature increase to 38% and 23 % by the end of the pulse. This is attributed to uncertainty accumulation, and it will affect the calculated conversions, which are sensitive to both electron density and electron temperature (see below). Moreover, the relative uncertainty in the afterglow is quite high for both electron density and temperature but the values are low, so it does not affect the calculation results to a large extent.

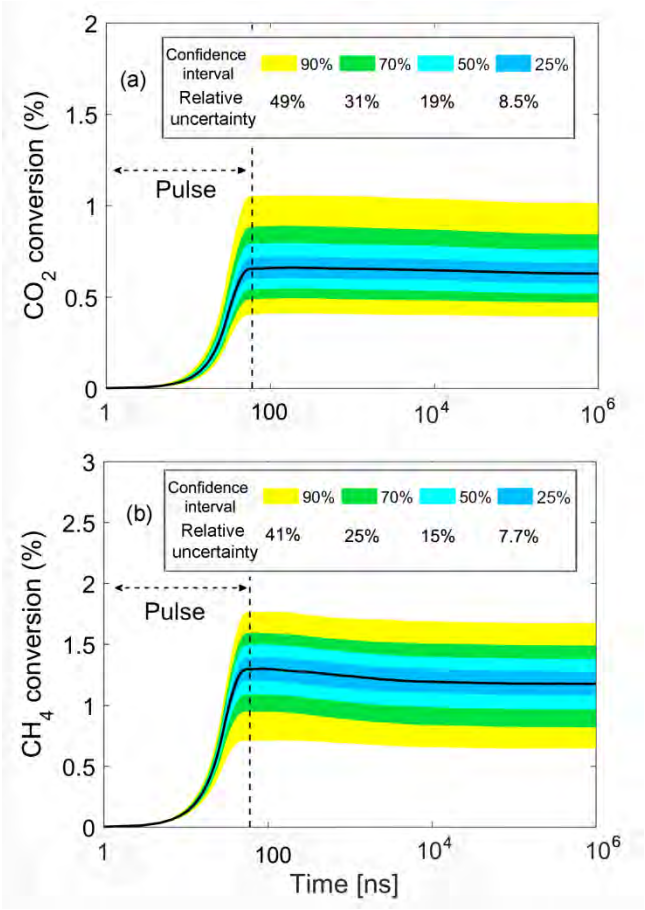

Figure 3 CO_2 conversion (a) and CH_4 conversion (b) as a function of time for one microdischarge pulse and afterglow. The vertical dashed line at t = 60 ns indicates the end of the microdischarge pulse. The median value is shown by the black curve. The different colours delimit different quantiles of the N = 2000 calculation results at each time, as indicated by the legend (see figure 2). The corresponding relative uncertainty (see legend) is now taken at the end of the microdischarge pulse.

The conversions of CO_2 and CH_4 are plotted as a function of time for one microdischarge pulse and afterglow in figure 3. The conversion rises during the pulse, mainly due to the electron impact dissociation reactions. CH_4 has a higher electron impact dissociation rate, leading to a more efficient conversion during the pulse. After the microdischarge pulse, the conversion of CO_2 stays constant, while the conversion of CH_4 exhibits a slight drop due to the recombination of CH_3 and H back to CH_4. After 10 μs, the CH_4 conversion reaches a steady state value as well, indicating that the production and loss processes compensate each other or have become all negligible. The uncertainties for the conversion of CO_2 and CH_4 are 31 % and 25 % at the end of the microdischarge pulse, for a confidence interval of 70%. For the other confidence intervals, they are presented in the legends. The

absolute uncertainties are listed in table 2. These relative uncertainties are larger than for the electron density and temperature, because they result from all the uncertainties of the quantities needed to calculate the conversions, including the rates of heavy particle reactions.

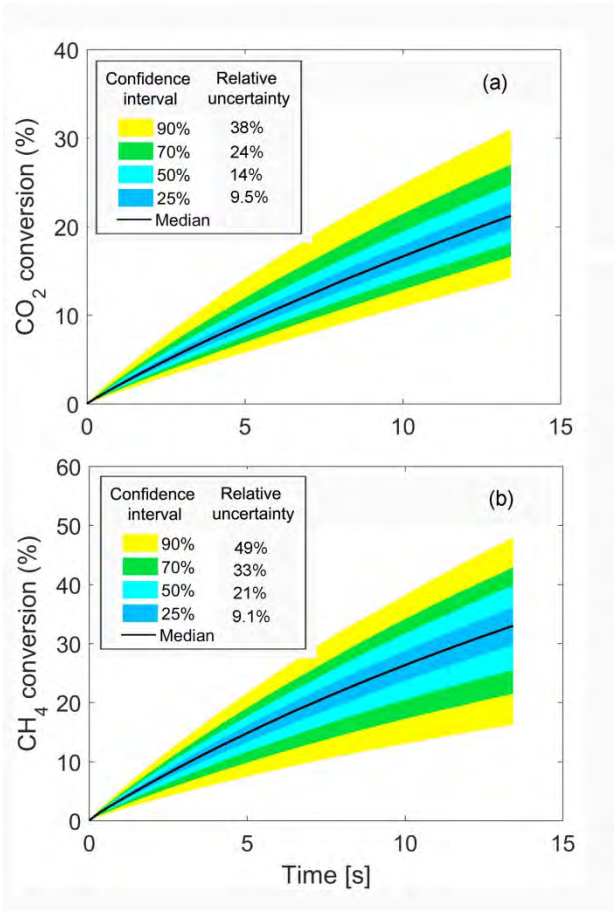

Figure 4 CO_2 conversion (a) and CH_4 conversion (b) as a function of time for the entire gas residence time in the plasma. The median value is shown by the black curve. The different colours delimit different quantiles of the N = 2000 calculation results at each time, as indicated by the legend. The corresponding relative uncertainty (see legend) is taken at the end of the residence time.

Figure 4 shows the calculated conversions of CO_2 and CH_4 as a function of time, for a total residence time of 13.7 s. The conversion of both gases increases more or less linearly with time. The relative uncertainties for the conversion of CO_2 and CH_4 are 24 % and 33% at the end of the gas residence time, for the 70% confidence interval. This corresponds to absolute uncertainties of 5% and 11%, respectively, i.e., the CO_2 and CH_4 conversions are calculated to be 21% ± 5%, and 33% ± 11% (see table 2). We should mention that in figure 4, we only present the calculated conversions of CO_2 and CH_4 at the end of each microdischarge pulse and afterglow. That is why no fluctuation in the conversions, like in figure 3, is observed for each pulse and afterglow.

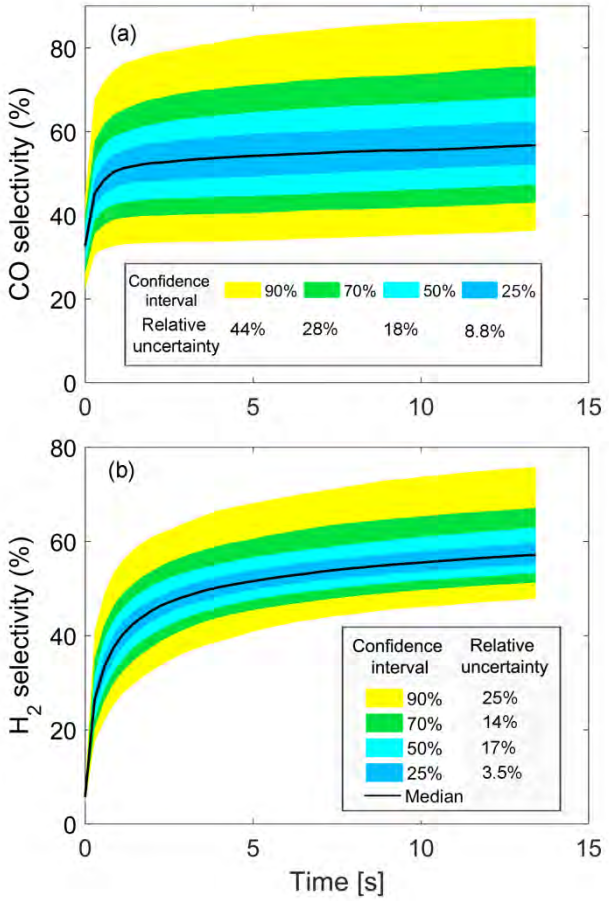

Figure 5 CO selectivity (a) and H_2 selectivity (b) as a function of time for the entire residence time. The median value is shown by the black curve. The different colours delimit different quantiles of the N = 2000 calculation results at each time, as indicated by the legend, and the corresponding relative uncertainty is taken at the end of the residence time.

The selectivities of the most important reaction products, i.e. H_2 and CO, increase drastically in a very short time scale in the beginning of the discharge, and reach both median values of 57% at the end of the gas residence time. This is in reasonable agreement with experimental data from literature at similar conditions [19]. The uncertainties in the CO and H_2 selectivities at the end of the residence time reach 28% and 14%, respectively, for the 70% confidence interval. In other words, the calculated selectivities are 57% ± 16% for CO, and 57% ± 8% for H_2 (see table 2).

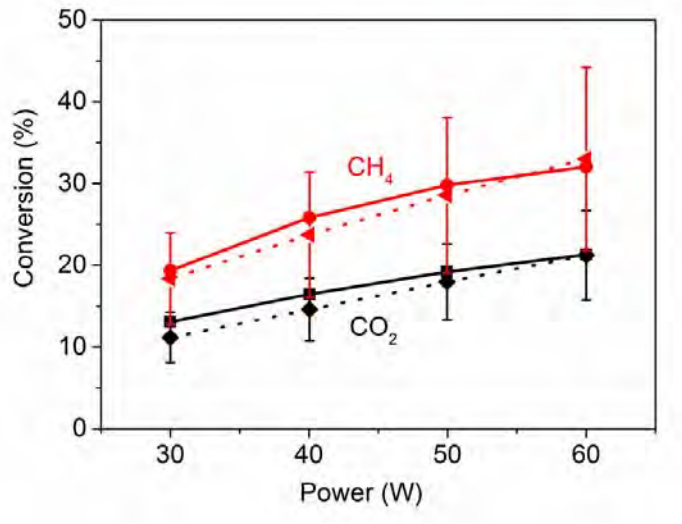

Figure 6 Calculated CO_2 and CH_4 conversion (median values) with error bars (i.e., absolute uncertainties) based on 70% confidence interval (dotted lines), in comparison to the measured data (solid lines; adopted from ref. [13] and [36]), in a 1:1 CO_2/CH_4 mixture at a total flow rate of 50 sccm, as a function of discharge power.

We also performed a similar uncertainty analysis for other conditions, and the median values of CO_2 and CH_4 conversion, calculated at the end of the gas residence time are plotted as a function of discharge power in figure 6, along with their error bars (or absolute uncertainties). We show again the comparison with the experimental values from ref. [13] and [36]. It is clear that the absolute uncertainties of the calculated CO_2 and CH_4 conversions increase with discharge power, but the relative uncertainties stay rather constant in the considered power range, i.e., around 25% and 32% for CO_2 and CH_4, respectively.

Note that this figure is very similar to figure 1 above, but now also including the error bars, indicating that the calculated data are in good agreement with the experimental values within the error bars. Indeed, in spite of the relatively large uncertainties in the calculated conversions, the trends in the calculations still agree with the experimental trends.

In principle, also the experimental error bars must be included, but they were not presented in ref. [13] (and the data of ref. [29] were adopted from ref. [13]). In our opinion, the error bars for both experimental and calculation results should always be presented, but this is seldom the case, especially for calculation results, which is of course understandable, keeping in mind the large effort needed to trace back the uncertainties of all input data and the large number of simulations required to obtain the uncertainties in the calculation results, as explained above.

3.2. Important reactions determining the uncertainties

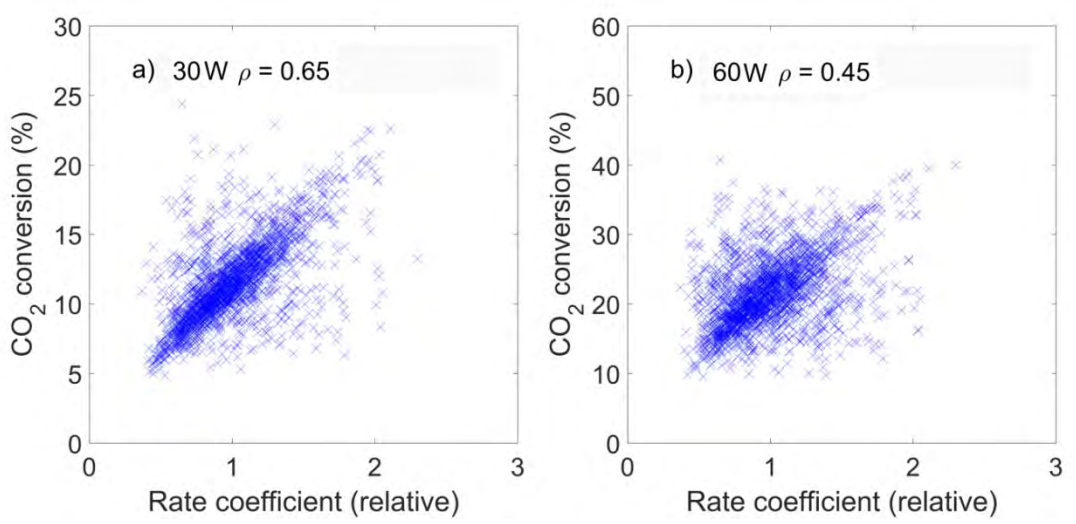

Figure 7 Scatter plot of the CO_2 conversion calculated with different values of the rate coefficient for electron impact CO_2 dissociation into CO and O (relative value with respect to the value listed in Table A.1, according to the tabulated uncertainty), for two different plasma powers. Each of the N = 2000 points corresponds to a simulation made with a different choice of this rate coefficient. The Spearman's ρ rank correlation coefficient is indicated in both cases (see text for explanation).

In order to identify the most important reactions affecting the uncertainty in the calculation results, we calculate the Spearman's rank correlation coefficients between the calculated properties and different reactions. For the CO_2 conversion, the largest Spearman's rank correlation coefficient is found for direct electron impact dissociation (X3 in Table A.1), showing that this reaction is the most significant CO_2 dissociation mechanism and also the dominant source of uncertainty for the CO_2 conversion in a DBD, in the power range considered in this work.

To grasp the concept of the Spearman's rank correlation coefficient, we show the calculated CO_2 conversion as a function of the rate coefficient for electron impact dissociation from ground state CO_2 (relative value with respect to the value listed in table A.1), for a plasma power of 30 W (figure 7 (a)) and 60 W (figure 7 (b)). Each data point in the scatter plot corresponds to one conversion data point and error bar, as also plotted in figure 4 and 6 above. The Spearman's rank correlation coefficient (ρ) is calculated to be 0.65 and 0.45, for a plasma power of 30 W and 60 W, respectively, thus indicating a more obvious correlation at the lower power.

We also checked the Spearman's rank correlation coefficients between the CO_2 conversion and the rate coefficients of other dominant reactions for the CO_2 conversion, and the result is plotted in figure 8 for a plasma power of 30 W and 60 W. At both power values, electron impact dissociation [X3] is, by far, the main source of uncertainty, while electron impact dissociative attachment [X2] is the second source of uncertainty. Indeed, although the relative contribution of reaction [X2] to the CO_2 conversion is below 5%, the uncertainty of this reaction changes the electron density, which affects the electron impact dissociation rate and hence the CO_2 conversion. No other significant correlations were found for the CO_2 conversion.

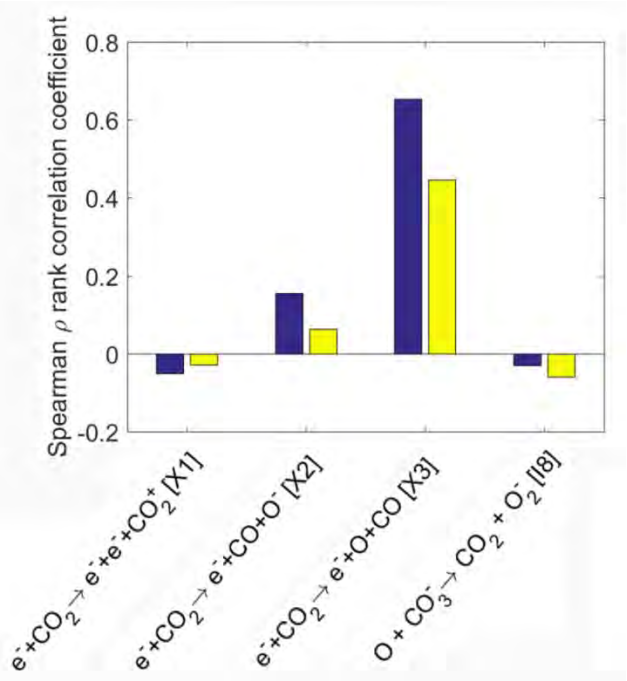

Figure 8 Spearman's ρ rank correlation coefficient between the calculated CO_2 conversion and the rate coefficients of different reactions, for a plasma power of 30 W (blue) and 60 W (yellow). The coefficients are only shown for the reactions having an influence on the CO_2 conversion.

Compared with the CO_2 conversion, the Spearman's rank correlation coefficient between the calculated CH_4 conversion and the (relative) rate coefficient of electron impact dissociation into CH_3 and H is much smaller, as presented in figure 9, with values of 0.23 and 0.16, for 30 W and 60 W, respectively. These smaller values of the Spearman's ρ rank correlation coefficient indicate that there exist other sources of uncertainty for the calculated CH_4 conversion.

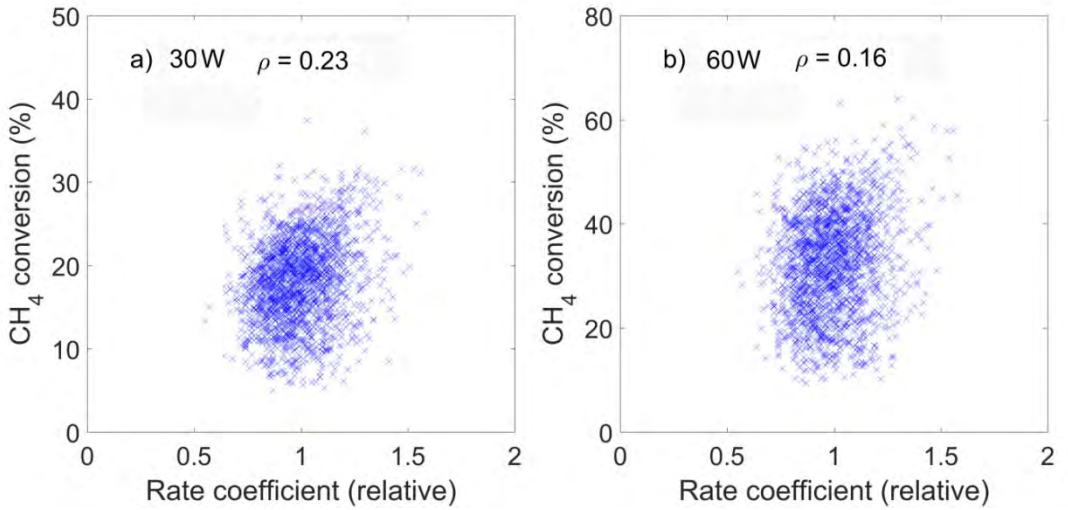

Figure 9 Scatter plot of the CH_4 conversion calculated with different values of the rate coefficient for electron impact CH_4 dissociation into CH_3 and H (relative value with respect to the value listed in Table A1, according to the tabulated uncertainty), for two different plasma powers. Each of the N = 2000 points corresponds to a simulation made with a different choice of this rate coefficient. The Spearman's ρ rank correlation coefficient is indicated in both cases.

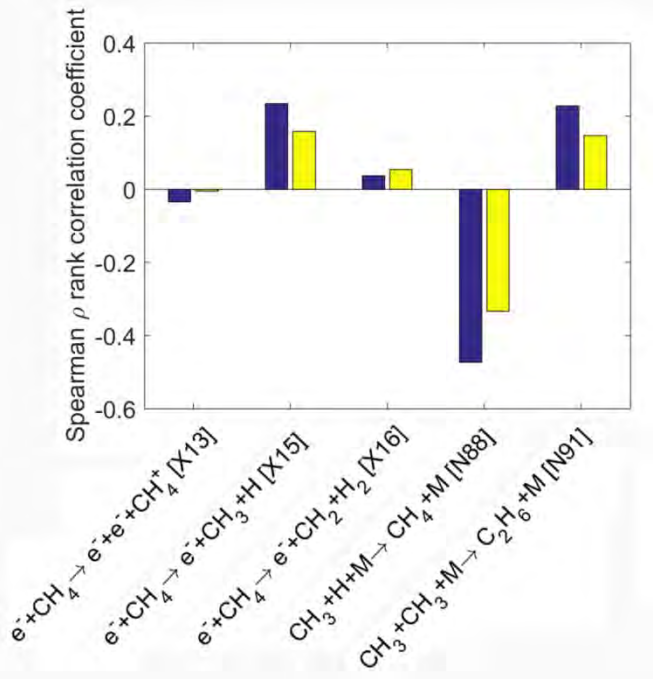

Figure 10 Spearman's ρ rank correlation coefficient between the calculated CH_4 conversion and the rate coefficients of different reactions, for a plasma power of 30 W (blue) and 60 W (yellow). The coefficients are only shown for the reactions having an influence on the CH_4 conversion.

Figure 10 shows the Spearman's ρ rank correlation coefficients between the calculated CH_4 conversion and the rate coefficients of the dominant reactions, having an influence on the CH_4 conversion. The largest absolute value of the Spearman's ρ rank correlation coefficient is obtained for the recombination reaction between CH_3 and H radicals back to CH_4 [N88]. For a plasma power of 30 W and 60 W, we obtain values of -0.47 and -0.33, respectively. The negative correlations show that increasing the rate coefficient for reaction [N88] hinders the conversion of CH_4. Indeed, reaction [N88] is the most significant process contributing to CH_4 formation. Besides, also reactions [X15] and [N91] shows a relatively large (positive) correlation with the calculated CH_4 conversion. For reaction [X15], this is like expected, being the dominant loss reaction for CH_4. However, reaction [N91] does not contribute to the formation and loss of CH_4. Nevertheless, this reaction can indirectly affect the CH_4 conversion, because of its competition in the consumption of CH_3 with reaction [N88]. Indeed, increasing the rate coefficient of reaction [N91] will indirectly promote the CH_4 conversion by inhibiting the recombination of CH_3 and H radicals back to CH_4 [N88]. This indicates how the uncertainty in rate coefficients of reactions which do not directly contribute to the CH_4 conversion, can still affect the uncertainty in the calculated CH_4 conversion.

As mentioned above, the syngas components (CO and H_2) are the main products of DRM. Therefore, we also analysed the Spearman's rank correlation coefficients between the calculated selectivities of CO and H_2 and the rate coefficients of different reactions, as presented in figure 11 and 12, in order to identify the main source of the uncertainties in the calculated CO and H_2 selectivities.

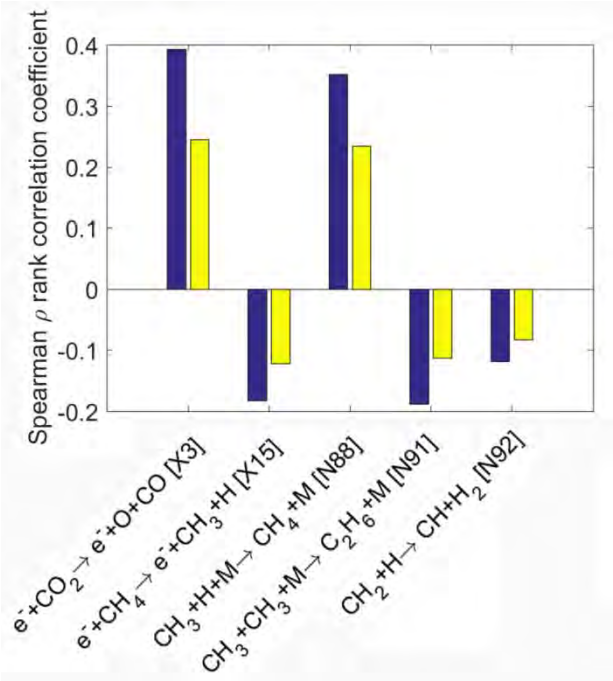

Figure 11 Spearman's ρ rank correlation coefficient between the calculated CO selectivity and the rate coefficients of different reactions, for a plasma power of 30 W (blue) and 60 W (yellow). The coefficients are only shown when the CO selectivity exhibits a clear dependence on the rate coefficient of the reaction, i.e. if $\rho > 0.1$ for one of the conditions.

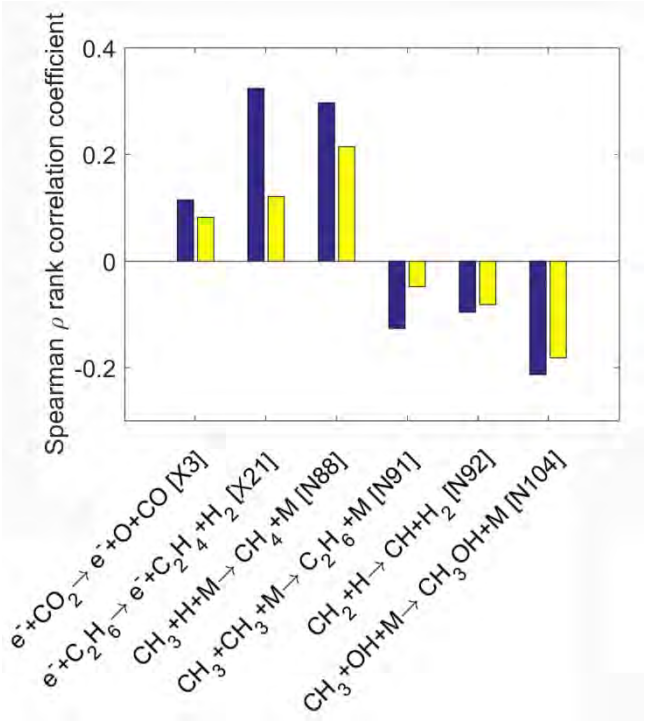

Figure 12 Spearman's ρ rank correlation coefficient between the calculated H_2 selectivity and the rate coefficients of different reactions, for a plasma power of 30 W (blue) and 60 W (yellow). The coefficients are only shown when the H_2 selectivity exhibits a clear dependence on the rate coefficient of the reaction, i.e. if $\rho > 0.1$ for one of the conditions.

For the CO selectivity, the largest uncertainty source comes from direct electron impact dissociation [X3], for which we obtain a Spearman's ρ rank correlation coefficient of 0.39 and 0.25,

for a plasma power of 30 W and 60 W, respectively. Indeed, this reaction [X3] is the most dominant mechanism for CO_2 conversion in a DBD plasma. The other reactions in figure 11, i.e., [X15], [N88], [N91] and [92], are not directly related to the CO_2 conversion. However, these reactions indirectly affect the CO selectivity by exerting some influence on the CH_4 conversion, explaining why we see clear correlations between the CO selectivity and the rate coefficients of these reactions ($\rho > 0.1$). For instance, reaction [X15] directly promotes the CH_4 conversion. This will not only produce syngas, but also hydrocarbons (C_xH_y) and oxygenates ($C_xH_yO_z$), which will reduce the CO selectivity, explaining the negative correlation of -0.18 and -0.12, at a plasma power of 30 W and 60 W, respectively. Reaction [N88] contributes to the formation of CH_4 and hence inhibits the conversion of CH_4 as well as the production of hydrocarbons and oxygenates, yielding a higher CO selectivity. The Spearman's ρ rank correlation coefficients for this reaction are 0.35 and 0.23, at a plasma power of 30 W and 60 W, respectively. Reaction [N91] shows negative correlations of -0.19 and -0.11, because it competes with reaction [N88] to consume CH_3 radicals and thus it promotes the conversion of CH_4 into hydrocarbons (mainly C_2H_6), reducing the CO selectivity. Finally, the reaction of CH_2 with H to form CH and H_2 [N88] reduces the CO selectivity, because most of the produced CH reacts back with CH_4 to generate C_2H_4 via reaction [N1], while some CH will destroy CO to produce CH_2O, both explaining the negative correlations of -0.11 and -0.08 with the CO selectivity.

For the H_2 selectivity, at a plasma power of 30 W, electron impact dissociation of C_2H_6 [X21] is the largest source of uncertainty ($\rho = 0.32$), because of its direct production of H_2. Reaction [N88], i.e. formation of CH_4 upon recombination between CH_3 and H, is the second source of uncertainty ($\rho =$ 0.30 at 30 W). Indeed, increasing the rate coefficient of reaction [N88] will inhibit the formation of higher hydrocarbons (C_xH_y) by consuming CH_3 radicals and hence decrease the H-based selectivity of higher hydrocarbons, and therefore increase the H_2 selectivity, regardless of the lower CH_4 conversion. In addition, reactions [N91], [N92] and [N104] also contribute to the uncertainty in the calculated H_2 selectivity. Indeed, they all have detrimental effect on the H_2 selectivity and hence give negative correlations. Reactions [N91] and [N104] produce C_2H_6 and CH_3OH, respectively, reducing the H_2 selectivity. Reaction [N92] produces H_2, but also CH, which reacts further with CH_4 to generate C_2H_4 via reaction [N1], compensating for the increase in H_2 selectivity by reaction [N92]. Comparing the results at 30 and 60 W, a higher power yields lower absolute correlations, both for the CO_2 and CH_4 conversions and the CO and H_2 selectivities. The reason is that more reactions play a role in determining the conversions and selectivities at higher power, hence distributing the correlation of the calculated conversions and selectivities over more reactions.

4. Conclusions

We evaluated the effect of uncertainties in the rate coefficients and cross sections on the calculation results for DRM in a DBD, by means of a zero-dimensional chemical kinetics model. For this purpose, we performed a detailed uncertainty analysis and sensitivity study. For each rate coefficient we calculated the probability of having a certain value from a log-normal distribution using the uncertainty reported for these rate coefficients. The latter is typically in the order of 10%–30%, but can rise up to 100% for reactions of charged species or even up to 1000% for neutral species reactions. Based on these probability distributions, we established 2000 different combinations of rate coefficients to predict the effect of their uncertainties on the calculated plasma properties, i.e. electron density, electron temperature, CO_2 and CH_4 conversion, as well as the selectivity of CO and H_2.

The uncertainties in the electron density and electron temperature are about 11 and 8%, respectively, at the maximum power deposition within one microdischarge pulse, for a 70% confidence interval, but they increase to 38 and 23% by the end of the pulse. These uncertainties greatly influence the CO_2 and CH_4 conversion, as well as the selectivity of CO and H_2. For the CO_2

and CH_4 conversion, we obtain uncertainties of 24% and 33%, respectively, for a 70% confidence level, while for the CO and H_2 selectivity, the uncertainties are 28% and 14%. These values were calculated for a typical power of 60 W, but similar results were obtained at other power values in the range of 30 – 60 W. In absolute terms, we can thus present our calculation results (for 60 W) as: N_e = (1.20 ± 0.11) $\times 10^{15}$ cm^{-3} and T_e= 2.60 ± 0.08 eV at the maximum of the microdischarge pulse, the overall CO_2 and CH_4 conversion at the end of the gas residence time are 21 ± 5 % and 33 ± 11 %, and the CO and H_2 selectivities are 57 ± 16 % and 57 ± 8 %, all determined for a 70% confidence interval. Hence, the absolute values of the calculation results suffer from relatively large uncertainties, but the predicted trends will probably still remain valid, and the model can still provide very useful information about the underlying chemical reaction kinetics [34].

We also calculated the Spearman's ρ rank correlation coefficients, to find correlations between the calculated plasma properties and the rate coefficients of the individual reactions. In this way, we can identify which reactions contribute most to the uncertainty in the model predictions. Direct electron impact dissociation is the dominant source of uncertainty for the CO_2 conversion. Electron impact dissociation of CH_4 (mainly into CH_3 and H), recombination of CH_3 and H back to CH_4, as well as the production of C_2H_6 via three-body recombination of CH_3, are the most significant contributions to the uncertainty of the CH_4 conversion, either by direct and indirect influence on the formation and loss of CH_4. All the above mentioned reactions also contribute to the uncertainty in the CO and H_2 selectivities.

It is clear that the uncertainties in the cross sections and rate coefficients can propagate and give relatively large uncertainties in the model output. In order to improve the accuracy and the reliability of chemical kinetics models, it is important to use verified rate coefficients, as also recommended by Turner [34] and by our group [37], and to validate the modelling results against experiments. For the latter, controlled experiments should be carried out in a simple design using controlled parameters, such as the gas temperature and the reduced electric field.

Finally, it is worth mentioning that the cross sections and rate coefficients are not the only source of uncertainty in the model. Other, more systematic uncertainties may arise from assumptions on the DBD filament properties in the model, such as the interpulse time and the microdischarge (pulse) duration. This was illustrated in our previous work, which also contributed to the verification and validation of chemical kinetic modelling results [40]. Also for these, experimental validation of the model results and assumptions is critically needed.

Acknowledgments

We acknowledge financial support from the Fund for Scientific Research Flanders (FWO) (grant no G.0383.16N) and the TOP-BOF project of the University of Antwerp. The calculations were carried out using the Turing HPC infrastructure at the CalcUA core facility of the Universiteit Antwerpen (UAntwerpen), a division of the Flemish Supercomputer Centre VSC, funded by the Hercules Foundation, the Flemish Government (department EWI) and the UAntwerpen.

Appendix. List of chemical reactions included in the model

Table A1. Electron impact reactions, as well as the references where the data are adopted from and the corresponding uncertainties (expressed relative to the mean value). These reactions are treated by energy-dependent cross sections. When not explicitly presented in the original source, the uncertainties in the reactions of electron impact upon CO_2 have been taken according to the values reported by Itikawa [51].

No.	Reaction	Ref.	Uncertainty $\Delta A/A$

X1[a]	$e^- + CO_2 \rightarrow e^- + e^- + CO_2^+$	[52]-[53]	0.10
X2[b]	$e^- + CO_2 \rightarrow CO + O^-$	[52]-[53]	0.30
X3[b]	$e^- + CO_2 \rightarrow e^- + CO + O$	[54]	0.30
X4[c]	$e^- + CO_2 \rightarrow e^- + CO_2(e1)$	[52]-[53]	0.30
X5[c]	$e^- + CO_2 \rightarrow e^- + CO_2(e2)$	[52]-[53]	0.30
X6	$e^- + CO \rightarrow e^- + e^- + CO^+$	[55]-[56]	0.10
X7	$e^- + CO \rightarrow e^- + C + O$	[55]-[56]	0.30
X8[b]	$e^- + O_2 \rightarrow e^- + O + O$	[57]	0.25
X9[b]	$e^- + O_2 \rightarrow O^- + O$	[57]	0.25
X10[b]	$e^- + O_2 + M \rightarrow O_2^- + M$	[57]	0.25
X11[c]	$e^- + O \rightarrow e^- + O(1D)$	[58]	0.20
X12[c]	$e^- + O \rightarrow e^- + O(1S)$	[58]	0.20
X13	$e^- + CH_4 \rightarrow e^- + e^- + CH_4^+$	[59]	0.15
X14	$e^- + CH_4 \rightarrow e^- + e^- + CH_3^+ + H$	[59]	0.15
X15	$e^- + CH_4 \rightarrow e^- + H + CH_3$	[60]-[61]	0.15
X16	$e^- + CH_4 \rightarrow e^- + H_2 + CH_2$	[60]-[61]	0.15
X17	$e^- + CH_4 \rightarrow e^- + CH + H_2 + H$	[60]-[61]	0.15
X18	$e^- + CH_4 \rightarrow e^- + C + 2H_2$	[60]-[61]	0.15
X19	$e^- + C_2H_6 \rightarrow e^- + e^- + C_2H_6^+$	[62]	0.20
X20	$e^- + C_2H_6 \rightarrow e^- + C_2H_5 + H$	[63]-[64]	0.75
X21	$e^- + C_2H_6 \rightarrow e^- + C_2H_4 + H_2$	[63]-[64]	0.75
X22	$e^- + C_2H_5 \rightarrow e^- + C_2H_4 + H$	[63]-[64]	0.75
X23	$e^- + C_2H_5 \rightarrow e^- + C_2H_3 + H_2$	[63]-[64]	0.75
X24	$e^- + C_2H_4 \rightarrow e^- + e^- + C_2H_4^+$	[62]	0.20
X25	$e^- + C_2H_4 \rightarrow e^- + C_2H_3 + H$	[63]-[64]	0.75
X26	$e^- + C_2H_4 \rightarrow e^- + C_2H_2 + H_2$	[63]-[64]	0.75
X27	$e^- + C_2H_3 \rightarrow e^- + C_2H_2 + H$	[63]-[64]	0.20
X28	$e^- + C_2H_2 \rightarrow e^- + e^- + C_2H_2^+$	[62]	0.75
X29	$e^- + C_3H_8 \rightarrow e^- + C_3H_7 + H$	[63]-[64]	0.75
X30	$e^- + C_3H_8 \rightarrow e^- + C_3H_6 + H_2$	[63]-[64]	0.75
X31	$e^- + C_3H_8 \rightarrow e^- + C_2H_4 + CH_4$	[63]-[64]	0.75
X32	$e^- + C_3H_7 \rightarrow e^- + C_3H_6 + H$	[63]-[64]	0.75
X33	$e^- + C_3H_7 \rightarrow e^- + C_2H_4 + CH_3$	[63]-[64]	0.75
X34	$e^- + C_3H_7 \rightarrow e^- + C_2H_3 + CH_4$	[63]-[64]	0.75
X35	$e^- + C_3H_6 \rightarrow e^- + C_2H_2 + CH_4$	[63]-[64]	0.75
X36[c]	$e^- + H_2 \rightarrow e^- + H_2(e)$	[63]-[64]	0.37
X37[c]	$e^- + H_2 \rightarrow e^- + H_2(v)$	[65]	0.20
X38[b],[d]	$e^- + H_2 \rightarrow e^- + H + H$	[65]	0.20
X39[a],[e]	$e^- + H_2 \rightarrow e^- + e^- + H_2^+$	[65]	0.07
X40[c]	$e^- + H \rightarrow e^- + H(2P)$	[66]	0.20
X41[a]	$e^- + H \rightarrow e^- + e^- + H^+$	[66]	0.10
X42[f]	$e^- + CH_3OH \rightarrow e^- + CH_3 + OH$	[67]	1.00
X43[f]	$e^- + CH_3OH \rightarrow e^- + CH_2OH + H$	[67]	1.00
X44[f]	$e^- + CH_3OH \rightarrow e^- + CH_3O + H$	[67]	1.00
X45	$e^- + H_2O \rightarrow O^- + H_2$	[68]	0.25
X46	$e^- + H_2O \rightarrow OH^- + H$	[68]	0.25
X47	$e^- + H_2O \rightarrow H^- + OH$	[68]	0.25
X48	$e^- + H_2O \rightarrow e^- + OH + H$	[68]	0.36
X49[c]	$e^- + O_2 \rightarrow e^- + O_2(a1)$	[57]	0.25
X50[c]	$e^- + O_2 \rightarrow e^- + O_2(b1)$	[57]	0.25
X51	$e^- + H^- \rightarrow e^- + e^- + H$	[69]	0.20
X52	$e^- + OH^- \rightarrow e^- + e^- + OH$	[70]	0.42

X53	$e^- + CH_3 \rightarrow e^- + CH_2 + H$	[60]-[61]	0.15
X54	$e^- + CH_2 \rightarrow e^- + CH + H$	[60]-[61]	0.15
X55	$e^- + C_2H_2 \rightarrow e^- + C_2H + H$	[63]-[64]	0.15

(a) Cross section also used for the electronically excited states, modified by lowering the energy threshold by the energy of the excited states.
(b) Same cross section also used for the electronically excited states.
(c) The cross sections for electron impact de-excitation are obtained from the excitation cross sections by the principle of detailed balance.
(d) Cross section also used for the vibrationally excited states, modified by lowering the energy threshold by the energy of the excited states.
(e) Same cross section also used for the vibrationally excited states.
(f) The primary source was not accessible and/or the uncertainty was not given, so we assume a value of 100%, which is large enough to check its influence.

Table A2. Electron impact reactions described by analytical expressions for the rate coefficients, given in cm^3/s and cm^6/s, for two-body and three-body reactions, respectively, as well as the references where the data are adopted from and the corresponding uncertainties (expressed relative to the mean value). T_g and T_e are given in K.

No.	Reaction	Rate coefficient	Ref.	Uncertainty $\Delta A/A$
E1[(a)]	$e^- + OH \rightarrow e^- + H + O$	2.5×10^{-8}	[71]	1.0
E2[(a)]	$e^- + OH^- \rightarrow e^- + e^- + O + H$	4.8×10^{-9}	[71]	1.0
E3	$e^- + O + M \rightarrow O^- + M$	1.0×10^{-31}	[72]	0.50
E4	$e^- + CO_2^+ \rightarrow CO + O$	$1.07 \times 10^{-3} T_e^{-0.50}/T_g$	[73]-[74]	0.08
E5	$e^- + CO_2^+ \rightarrow C + O_2$	$1.07 \times 10^{-3} T_e^{-0.50}/T_g$	[73]-[74]	0.08
E6[(a)]	$e^- + CO_4^+ \rightarrow CO_2 + O_2$	$1.73 \times 10^{-5} T_e^{-0.50}$	[75]	0.30
E7	$e^- + CO^+ \rightarrow C + O$	$2.0 \times 10^{-7} (T_e/300)^{-0.48}$	[76]-[77]	0.25
E8[(a)]	$e^- + C_2O_4^+ \rightarrow CO_2 + CO_2$	$2.15 \times 10^{-3} T_e^{-0.50}/T_g$	[78]	0.50
E9	$e^- + CH_5^+ \rightarrow CH_3 + 2H$	$2.57 \times 10^{-7} (T_e/300)^{-0.30}$	[60],[79]	0.15
E10	$e^- + CH_5^+ \rightarrow CH_2 + H_2 + H$	$6.61 \times 10^{-8} (T_e/300)^{-0.30}$	[60],[79]	0.15
E11	$e^- + C_2H_5^+ \rightarrow C_2H_4 + H$	$7.70 \times 10^{-8} (T_e/300)^{-0.71}$	[64]	0.15
E12	$e^- + C_2H_5^+ \rightarrow C_2H_3 + 2H$	$1.92 \times 10^{-8} (T_e/300)^{-0.71}$	[64]	0.15
E13	$e^- + C_2H_5^+ \rightarrow C_2H_2 + H_2 + H$	$1.60 \times 10^{-8} (T_e/300)^{-0.71}$	[64]	0.15
E14	$e^- + C_2H_5^+ \rightarrow C_2H_2 + 3H$	$8.98 \times 10^{-9} (T_g/300)^{-0.71}$	[64]	0.15
E15	$e^- + C_2H_4^+ \rightarrow C_2H_2 + 2H$	$3.43 \times 10^{-8} (T_e/300)^{-0.71}$	[64]	0.15
E16[(a)]	$e^- + C_2O_2^+ \rightarrow CO + CO$	$1.39 \times 10^{-6} (T_e/300)^{-0.34}$	[78]	0.50
E17	$e^- + H_3O^+ \rightarrow H_2O + H$	$7.09 \times 10^{-8} (T_e/300)^{-0.50}$	[80]	0.20
E18	$e^- + H_3O^+ \rightarrow H_2 + OH$	$5.37 \times 10^{-8} (T_e/300)^{-0.50}$	[80]	0.20
E19	$e^- + H_3O^+ \rightarrow 2H + OH$	$3.05 \times 10^{-7} (T_e/300)^{-0.50}$	[80]	0.20
E20	$e^- + CH_4^+ \rightarrow CH_3 + H$	$1.18 \times 10^{-8} (T_e/300)^{-0.50}$	[60],[79]	0.15
E21	$e^- + CH_4^+ \rightarrow CH_2 + 2H$	$2.42 \times 10^{-8} (T_e/300)^{-0.50}$	[60],[79]	0.15
E22	$e^- + CH_4^+ \rightarrow CH + H_2 + H$	$1.41 \times 10^{-8} (T_e/300)^{-0.50}$	[60],[79]	0.15
E23	$e^- + CH_3^+ \rightarrow CH_2 + H$	$2.25 \times 10^{-8} (T_e/300)^{-0.50}$	[60],[79]	0.15
E24	$e^- + CH_3^+ \rightarrow CH + H_2$	$7.88 \times 10^{-9} (T_e/300)^{-0.50}$	[60],[79]	0.15
E25	$e^- + CH_3^+ \rightarrow CH + 2H$	$9.00 \times 10^{-9} (T_e/300)^{-0.50}$	[60],[79]	0.15
E26	$e^- + CH_3^+ \rightarrow C + H + H_2$	$1.69 \times 10^{-8} (T_e/300)^{-0.50}$	[60],[79]	0.15
E27	$e^- + C_2H_6^+ \rightarrow C_2H_5 + H$	$2.19 \times 10^{-8} (T_e/300)^{-0.71}$	[64]	0.15
E28	$e^- + C_2H_6^+ \rightarrow C_2H_4 + 2H$	$3.36 \times 10^{-8} (T_e/300)^{-0.71}$	[64]	0.15

E29	$e^- + C_2H_3^+ \rightarrow C_2H_2 + H$	$2.74 \times 10^{-8}(T_e/300)^{-0.71}$	[64]	0.15
E30	$e^- + C_2H_2^+ \rightarrow CH + CH$	$1.87 \times 10^{-8}(T_e/300)^{-0.71}$	[64]	0.15
E31[(a)]	$e^- + C_2O_3^+ \rightarrow CO_2 + CO$	$3.78 \times 10^{-5}T_e^{-0.70}$	[78]	0.50
E32[(a)]	$e^- + H^+ \rightarrow H$	3.52×10^{-13}	[81]	0.50
E33[(a)]	$e^- + H_2^+ \rightarrow 2H$	$5.33 \times 10^{-8}(T_g/300)^{-0.40}$	[81]	0.50

(a) The primary source was not accessible and/or the uncertainty was not given, so the uncertainty was assumed based on the dispersion of the literature data.

Table A3. Ion-ion and ion-neutral reactions, as well as the references where the data are adopted from and the corresponding uncertainties (expressed relative to the mean value). The rate coefficients are given in cm^3/s and cm^6/s, for two-body and three-body reactions, respectively. T_g is given in K.

No.	Reaction	Rate coefficient	Ref.	Uncertainty $\Delta A/A$
I1	$CO_2 + CO^+ \rightarrow CO_2^+ + CO$	1.0×10^{-9}	[82]-[83]	0.20
I2[(a)]	$CO_2 + O^- + M \rightarrow CO_3^- + M$	9.0×10^{-29}	[84]	1.00
I3[(a)]	$CO_2 + O_2^- + M \rightarrow CO_4^- + M$	1.0×10^{-29}	[84]	1.00
I4	$CO_2 + O_3^- \rightarrow CO_3^- + O_2^-$	5.5×10^{-10}	[82],[85]	0.30
I5[(a)]	$CO_2 + CO_2^+ + M \rightarrow C_2O_4^+ + M$	3.0×10^{-28}	[78]	1.00
I6	$CO + O^- + M \rightarrow CO_2 + e^-$	5.5×10^{-10}	[85]	0.30
I7[(a)]	$CO + CO_3^- \rightarrow 2CO_2 + e^-$	5.5×10^{-17}	[84]	1.00
I8[(a)]	$O + CO_3^- \rightarrow O_2^- + CO_2$	8.0×10^{-11}	[85]	1.00
I9[(a)]	$O + CO_4^- \rightarrow CO_3^- + O_2$	1.1×10^{-10}	[82]	1.00
I10[(a)]	$O + CO_4^- \rightarrow CO_2 + O^- + O_2$	1.4×10^{-11}	[82]	1.00
I11[(a)]	$O + CO_4^- \rightarrow CO_2 + O^- + O_2$	1.4×10^{-11}	[82]	1.00
I12[(a)]	$CO + C_2O_3^+ + M \rightarrow C_2O_2^+ + CO_2 + M$	2.6×10^{-26}	[78]	1.00
I13[(a)]	$CO + C_2O_4^+ + M \rightarrow C_2O_3^+ + CO_2 + M$	4.2×10^{-26}	[78]	1.00
I14[(a)]	$CH_5^+ + C_2H_6 \rightarrow C_2H_5^+ + H_2 + CH_4$	2.3×10^{-10}	[87]	1.00
I15[(a)]	$CH_5^+ + C_2H_4 \rightarrow C_2H_5^+ + CH_4$	1.5×10^{-9}	[79]	1.00
I16[(a)]	$CH_5^+ + C_2H_2 \rightarrow C_2H_3^+ + CH_4$	1.6×10^{-9}	[79]	1.00
I17[(a)]	$CH_4^+ + CH_4 \rightarrow CH_5^+ + CH_3$	1.5×10^{-9}	[79]	1.00
I18[(a)]	$CH_4^+ + C_2H_6 \rightarrow C_2H_4^+ + CH_4 + H_2$	1.9×10^{-9}	[87]	1.00
I19[(a)]	$CH_3^+ + CH_4 \rightarrow CH_4^+ + CH_3$	1.7×10^{-10}	[88]	1.00
I20[(a)]	$CH_3^+ + CH_4 \rightarrow C_2H_5^+ + H_2$	1.2×10^{-9}	[79]	1.00
I21[(a)]	$C_2H_4^+ + H \rightarrow C_2H_3^+ + H_2$	3.0×10^{-10}	[79]	1.00
I22[(a)]	$C_2H_3^+ + C_2H_4 \rightarrow C_2H_5^+ + C_2H_2$	8.9×10^{-10}	[79]	1.00
I23[(a)]	$H_2^+ + CH_4 \rightarrow CH_3^+ + H_2 + H$	2.3×10^{-9}	[79]	1.00
I24[(a)]	$H^+ + CH_4 \rightarrow CH_4^+ + H$	1.5×10^{-9}	[79]	1.00
I25[(a)]	$H^- + H \rightarrow H_2 + e^-$	1.3×10^{-9}	[79]	1.00
I26[(a)]	$CH_5^+ + H_2O \rightarrow H_3O^+ + CH_4$	$3.7 \times 10^{-9}(T_g/300)^{-0.50}$	[79]	1.00
I27[(a)]	$CH_4^+ + H_2O \rightarrow H_3O^+ + CH_3$	$2.6 \times 10^{-9}(T_g/300)^{-0.50}$	[79]	1.00
I28[(a)]	$C_2H_6^+ + H_2O \rightarrow H_3O^+ + C_2H_5$	$3.0 \times 10^{-9}(T_g/300)^{-0.50}$	[79]	1.00
I29[(a)]	$C_2H_5^+ + H_2O \rightarrow H_3O^+ + C_2H_4$	$1.4 \times 10^{-9}(T_g/300)^{-0.50}$	[79]	1.00
I30[(a)]	$C_2H_3^+ + H_2O \rightarrow H_3O^+ + C_2H_2$	$1.1 \times 10^{-9}(T_g/300)^{-0.50}$	[79]	1.00
I31[(a)]	$H^- + H_2O \rightarrow H_2 + OH^-$	3.8×10^{-9}	[79]	1.00
I32[(a)]	$O^- + CH_4 \rightarrow CH_3 + OH^-$	1.0×10^{-10}	[79]	1.00
I33[(a)]	$O^- + H_2 \rightarrow H_2O + e^-$	7.0×10^{-10}	[79]	1.00
I34[(a)]	$CO_2^+ + CH_4 \rightarrow CH_4^+ + CO_2$	5.0×10^{-10}	[79]	1.00
I35[(a)]	$CO + CH_4 \rightarrow CH_4^+ + CO$	7.9×10^{-10}	[79]	1.00
I36[(a)]	$OH^- + H \rightarrow H_2O + e^-$	1.4×10^{-9}	[79]	1.00

I37[(a)]	$O_3^- + M \rightarrow M + O_3 + e^-$	2.4×10^{-11}	[89]	1.00
I38[(a)]	$H_3O^+ + CO_3^- \rightarrow H_2O + H + CO_2 + O$	1.0×10^{-7}	[90]	0.50
I39[(a)]	$H_3O^+ + CO_4^- \rightarrow H_2O + H + CO_2 + O_2$	1.0×10^{-7}	[90]	0.50
I40[(a)]	$CO_2^+ + CO_3^- \rightarrow 2CO_2 + O$	5.0×10^{-7}	[74]	0.50
I41[(a)]	$CO_2^+ + CO_4^- \rightarrow 2CO_2 + O_2$	5.0×10^{-7}	[74]	0.50
I42[(a)]	$C_2O_2^+ + CO_3^- \rightarrow CO_2 + 2CO + O$	5.0×10^{-7}	[74]	0.50
I43[(a)]	$C_2O_2^+ + CO_4^- \rightarrow CO_2 + 2CO + O_2$	5.0×10^{-7}	[74]	0.50

(a) The primary source was not accessible and/or the uncertainty was not given, so the uncertainty was assumed based on the dispersion of the literature data.

Table A4. Neutral-neutral reactions, as well as the references where the data are adopted from and the corresponding uncertainties (expressed relative to the mean value). The rate coefficients are given in cm^3/s and cm^6/s, for two-body and three-body reactions, respectively. T_g is given in K.

No.	Reaction	Rate coefficient	Ref.	Uncertainty $\Delta A/A$
N1	$CH_4 + CH \rightarrow C_2H_4 + H$	9.97×10^{-11}	[91]	10.0
N2	$CH_3 + CH_2 \rightarrow C_2H_4 + H$	7.01×10^{-11}	[92]	3.16
N3[(a)]	$CH_3 + C_2H_5 + M \rightarrow C_3H_8 + M$	5.00×10^{-29}	[34]	3.00
N4	$CH_2 + C_2H_5 \rightarrow C_2H_4 + CH_3$	3.01×10^{-11}	[91]	3.00
N5	$CH_2 + C_2H_3 \rightarrow C_2H_2 + CH_3$	3.01×10^{-11}	[91]	10.0
N6	$CH + C_2H_6 + M \rightarrow C_3H_7 + M$	1.14×10^{-29}	[92]	10.0
N7[(a)]	$C + H_2 \rightarrow CH + H$	1.50×10^{-10}	[93]	10.0
N8	$C_2H_5 + C_2H_5 \rightarrow C_2H_6 + C_2H_4$	2.41×10^{-12}	[92]	2.51
N9	$C_2H_5 + C_3H_7 \rightarrow C_3H_8 + C_2H_4$	1.91×10^{-12}	[94]	1.40
N10	$C_2H_5 + C_3H_7 \rightarrow C_3H_6 + C_2H_6$	2.41×10^{-12}	[94]	1.40
N11	$C_2H_5 + H \rightarrow CH_3 + CH_3$	5.99×10^{-11}	[92]	2.00
N12	$C_2H_5 + H \rightarrow C_2H_4 + H_2$	3.01×10^{-12}	[91]	3.00
N13[(a)]	$C_2H_5 + H \rightarrow C_2H_6$	6.00×10^{-11}	[95]	10.0
N14	$C_2H_3 + H \rightarrow C_2H_2 + H_2$	2.01×10^{-11}	[92]	3.16
N15[(a)]	$C_2H_3 + H + M \rightarrow C_2H_4 + M$	8.26×10^{-30}	[96]	2.00
N16[(a)]	$C_2H_6 + CH_2 \rightarrow C_3H_8$	4.80×10^{-12}	[97]	2.00
N17	$H + H + M \rightarrow H_2 + M$	6.00×10^{-33}	[92]	3.16
N18[(a)]	$H_2(v) + H_2 \rightarrow H_2 + H_2$	1.00×10^{-13}	[81]	10.0
N19[(a)]	$H_2(e) + H_2 \rightarrow H_2 + H_2$	1.00×10^{-13}	[81]	10.0
N20	$CH_3 + O \rightarrow CH_2O + H$	1.40×10^{-10}	[92]	1.58
N21	$CH_3 + O \rightarrow CO + H_2 + H$	5.68×10^{-11}	[98]	1.58
N22	$CH_2 + O \rightarrow CO + H_2$	5.53×10^{-11}	[98]	0.30
N23	$CH_2 + O \rightarrow CO + 2H$	8.29×10^{-11}	[98]	0.30
N24[(a)]	$CH_2 + O \rightarrow CHO + H$	5.01×10^{-11}	[98]	2.00
N25	$C_2H_5 + O \rightarrow CH_3CHO + H$	8.80×10^{-11}	[98]	0.05
N26	$C_2H_5 + O \rightarrow CH_2O + CH_3$	6.60×10^{-11}	[98]	0.10
N27	$C_2H_5 + O \rightarrow C_2H_4 + OH$	4.40×10^{-11}	[98]	0.10
N28	$C_2H_4 + O \rightarrow CH_2CHO + H$	2.63×10^{-13}	[98]	0.05
N29	$C_2H_4 + O \rightarrow CHO + CH_3$	4.51×10^{-13}	[98]	0.10
N30	$C_2H_3 + O \rightarrow C_2H_2 + OH$	1.25×10^{-11}	[91]	0.50
N31	$C_2H_3 + O \rightarrow CO + CH_3$	1.25×10^{-11}	[91]	0.50
N32	$C_2H_3 + O \rightarrow CHO + CH_2$	1.25×10^{-11}	[91]	0.50
N33	$C_2H_3 + O \rightarrow CH_2CO + H$	1.60×10^{-10}	[91]	3.00
N34	$C_2H_3 + O_2 \rightarrow CH_2O + CHO$	9.00×10^{-12}	[92]	3.16
N35	$H + O_3 \rightarrow OH + O_2$	2.86×10^{-11}	[99]	2.00

N36	$CH_2 + CO_2 \rightarrow CH_2O + CO$	3.90×10^{-14}	[91]	1.60
N37	$CH_2 + OH \rightarrow CH_2O + H$	3.00×10^{-11}	[91]	3.00
N38	$CH + CO_2 \rightarrow CHO + CO$	9.68×10^{-13}	[98]	0.15
N39	$CH + CO_2 \rightarrow 2CO + H$	9.68×10^{-13}	[98]	0.15
N40	$C_2H_5 + OH \rightarrow C_2H_4 + H_2O$	4.00×10^{-11}	[91]	5.00
N41	$C_2H_5 + CHO \rightarrow C_2H_6 + CO$	2.01×10^{-10}	[91]	3.00
N42	$C_2H_5 + CH_3O \rightarrow C_2H_6 + CH_2O$	4.00×10^{-11}	[91]	5.00
N43	$C_2H_3 + OH \rightarrow C_2H_2 + H_2O$	5.00×10^{-11}	[91]	3.00
N44	$C_2H_3 + CHO \rightarrow C_2H_4 + CO$	1.50×10^{-10}	[91]	3.00
N45	$C_2H_3 + CH_3O \rightarrow C_2H_4 + CH_2O$	4.00×10^{-11}	[91]	5.00
N46	$H + CHO \rightarrow CO + H_2$	3.32×10^{-10}	[100]	2.00
N47	$H + CH_3O \rightarrow H_2 + CH_2O$	2.32×10^{-11}	[98]	0.20
N48	$H + CH_3O \rightarrow CH_3 + OH$	9.93×10^{-12}	[98]	0.20
N49	$H + CH_3CHO \rightarrow H_2 + CH_3CO$	8.98×10^{-14}	[92]	0.10
N50	$H + CH_2CO \rightarrow CH_3 + CO$	1.04×10^{-13}	[92]	0.50
N51	$H + C_2HO \rightarrow CH_2 + CO$	2.50×10^{-10}	[92]	0.40
N52	$O + CHO \rightarrow CO + OH$	5.00×10^{-11}	[92]	2.00
N53	$O + CHO \rightarrow H + CO_2$	5.00×10^{-11}	[92]	2.00
N54 [(a)]	$O + CH_2O \rightarrow CH_2 + CO_2$	2.29×10^{-13}	[101]	2.00
N55	$CO + OH \rightarrow CO_2 + H$	1.25×10^{-13}	[92]	3.16
N56	$CHO + OH \rightarrow CO + H_2O$	1.69×10^{-10}	[92]	2.00
N57	$OH + CH_3CHO \rightarrow CH_3CO + H_2O$	1.57×10^{-11}	[99]	1.26
N58	$OH + CH_2CO \rightarrow CO + CH_2OH$	1.70×10^{-11}	[92]	1.00
N59	$C_2H_5O_2 + C_2H_5O_2 \rightarrow C_2H_5OH + CH_3CHO + O_2$	2.43×10^{-14}	[102]	0.12
N60	$C_2H_5O_2 + C_2H_5O_2 \rightarrow 2C_2H_5O + O_2$	3.97×10^{-14}	[102]	0.12
N61	$CH_2 + CH_3CO \rightarrow CH_2CO + CH_3$	3.00×10^{-11}	[91]	3.00
N62	$C_2H_5 + CH_2OH \rightarrow C_2H_6 + CH_2O$	4.00×10^{-12}	[103]	5.00
N63	$C_2H_5 + CH_2OH \rightarrow CH_3OH + C_2H_4$	4.00×10^{-12}	[103]	5.00
N64	$C_2H_3 + CH_2OH \rightarrow C_2H_4 + CH_2O$	5.00×10^{-11}	[103]	5.00
N65	$H + CH_2OH \rightarrow CH_2O + H_2$	1.00×10^{-11}	[103]	2.50
N66	$H + CH_2OH \rightarrow CH_3 + OH$	1.60×10^{-10}	[103]	2.00
N67	$O + CH_3O \rightarrow CH_2CO + OH$	8.75×10^{-11}	[98]	0.20
N68	$O + CH_3O \rightarrow CO_2 + CH_3$	2.63×10^{-10}	[98]	0.20
N69	$O + CH_2OH \rightarrow CH_2O + OH$	7.00×10^{-11}	[103]	2.00
N70	$O_2 + C_2H_5O \rightarrow CH_3CHO + HO_2$	8.12×10^{-15}	[102]	1.58
N71	$OH + CH_3CO \rightarrow CH_2CO + H_2O$	2.00×10^{-11}	[91]	3.00
N72	$OH + CH_3CO \rightarrow CH_3 + CO + OH$	5.00×10^{-11}	[91]	3.00
N73	$HO_2 + CH_3CO \rightarrow CH_3 + CO_2 + OH$	5.00×10^{-11}	[91]	3.00
N74	$CH_3O + CH_3CO \rightarrow CH_3OH + CH_2CO$	1.00×10^{-11}	[91]	5.00
N75	$C_2H_5 + O_2 \rightarrow C_2H_5O_2$	5.00×10^{-12}	[99]	2.00
N76 [(a)]	$O(1D) + CH_4 \rightarrow CH_3 + OH$	3.11×10^{-10}	[104]	5.00
N77 [(a)]	$O(1D) + CH_4 \rightarrow CH_3OH$	4.98×10^{-11}	[105]	5.00
N78 [(a)]	$O(1D) + CH_4 \rightarrow CH_2OH + H$	6.90×10^{-12}	[106]-[107]	5.00
N79 [(a)]	$O(1D) + CO \rightarrow CO_2$	8.00×10^{-11}	[108]	2.00
N80 [(a)]	$O(1D) + CO \rightarrow CO + O$	5.00×10^{-11}	[109]	0.50
N81 [(a)]	$CH_2O + O \rightarrow CO + OH + H$	1.00×10^{-10}	[110]	5.00
N82 [(a)]	$O_2(b1) + O_3 \rightarrow O_2 + O_2 + O$	2.20×10^{-11}	[111]	2.00
N83 [(a)]	$O(1S) + O_2(a1) \rightarrow O(1D) + O_2(b1)$	2.90×10^{-11}	[111]	2.00
N84 [(a)]	$O(1S) + O_2(a1) \rightarrow 3O$	3.20×10^{-11}	[111]	2.00

N85	$O(1D) + H_2O \rightarrow 2OH$	2.20×10^{-10}	[112]	1.26
N86 [(a)]	$CO_2(e1) + M \rightarrow CO_2 + M$	1.00×10^{-11}	[45]	2.00
N87 [(a)]	$CO_2(e2) + M \rightarrow CO_2 + M$	1.00×10^{-11}	[45]	2.00
N88	$CH_3 + H + M \rightarrow CH_4 + M$	$3.01 \times 10^{-28} (T_g/298)^{-1.80}$	[92]	2.00
N89	$CH_2 + CH_2 \rightarrow C_2H_2 + 2H$	$3.32 \times 10^{-10} \exp(-5530.4/T_g)$	[113]	2.00
N90	$CH_2 + CH_2 \rightarrow C_2H_2 + H_2$	$9.98 \times 10^{-12} T_g^{0.5}$	[114]	1.58
N91	$CH_3 + CH_3 + M \rightarrow C_2H_6 + M$	$1.68 \times 10^{-24} (T_g/298)^{-7.0} \exp(-1390.4/T_g)$	[92]	10.0
N92	$CH_2 + H \rightarrow CH + H_2$	$1.00 \times 10^{-11} \exp(899.7/T_g)$	[92]	10.0
N93 [(a)]	$CH + H \rightarrow C + H_2$	$1.31 \times 10^{-10} \exp(-805.9/T_g)$	[115]	3.00
N94	$C_2H_4 + H + M \rightarrow C_2H_5 + M$	$7.69 \times 10^{-30} \exp(-380.1/T_g)$	[116]	2.00
N95	$C_2H_2 + H + M \rightarrow C_2H_3 + M$	$1.08 \times 10^{-25} (T_g/298)^{-7.27} \exp(-3630.0/T_g)$	[92]	2.00
N96	$C_3H_7 + H \rightarrow C_3H_8$	$9.67 \times 10^{-11} (T_g/298)^{0.22}$	[117]	2.00
N97 [(a)]	$O + O + M \rightarrow O_2 + M$	$1.27 \times 10^{-32} (T_g/298)^{-1.0} \exp(-170.0/T_g)$	[118]	10.0
N98 [(a)]	$O(1S) + O \rightarrow O(1D) + O$	$5.00 \times 10^{-11} \exp(-300.0/T_g)$	[111]	10.0
N99	$C_2H_2 + O \rightarrow CH_2 + CO$	$1.53 \times 10^{-13} (T_g/298)^{2.80} \exp(-250.2/T_g)$	[92]	1.58
N100	$C_2H_2 + O \rightarrow C_2HO + H$	$1.53 \times 10^{-13} (T_g/298)^{2.80} \exp(-250.2/T_g)$	[92]	1.58
N101	$H + O + M \rightarrow OH + M$	$4.36 \times 10^{-32} (T_g/298)^{-1.0}$	[91]	5.00
N102	$H + O_2 + M \rightarrow HO_2 + M$	$6.09 \times 10^{-32} (T_g/298)^{-0.80}$	[116]	3.16
N103	$CH_4 + OH \rightarrow CH_3 + H_2O$	$1.36 \times 10^{-13} (T_g/298)^{3.04} \exp(-920.1/T_g)$	[119]	1.20
N104[(a)]	$CH_3 + OH + M \rightarrow CH_3OH + M$	$3.69 \times 10^{-29} \exp(1279.8/T_g)$	[120]	2.00
N105	$CH + CO + M \rightarrow C_2HO + M$	$4.15 \times 10^{-30} (T_g/298)^{-1.90}$	[98]	0.30
N106	$C_2H_6 + OH \rightarrow C_2H_5$	$1.06 \times 10^{-12} (T_g/298)^{2.0} \exp(-435.0/T_g)$	[92]	1.41
N107	$H + CO + M \rightarrow CHO + M$	$1.90 \times 10^{-33} \exp(-842.0/T_g)$	[100]	1.58
N108	$H + OH + M \rightarrow H_2O + M$	$4.33 \times 10^{-30} (T_g/298)^{-2.0}$	[92]	2.00
N109	$H + HO_2 \rightarrow H_2O + O$	$8.30 \times 10^{-11} \exp(-502.8/T_g)$	[121]	3.16
N110	$H + HO_2 \rightarrow OH + OH$	$2.81 \times 10^{-10} \exp(-440.2/T_g)$	[122]	2.00
N111	$H + HO_2 \rightarrow O_2 + H_2$	$4.15 \times 10^{-11} \exp(-248.8/T_g)$	[122]	1.58
N112[(a)]	$O + OH \rightarrow O_2 + H$	$4.55 \times 10^{-12} (T_g/298)^{0.40} \exp(-371.7/T_g)$	[123]	3.00
N113	$O + HO_2 \rightarrow O_2 + OH$	$1.36 \times 10^{-11} (T_g/298)^{0.75}$	[124]	5.00
N114[(a)]	$O + CH_3O \rightarrow O_2 + CH_3$	$3.55 \times 10^{-11} \exp(-239.3/T_g)$	[125]	2.00
N115	$O + CH_3CHO \rightarrow OH + CH_3CO$	$8.30 \times 10^{-12} \exp(-902.1/T_g)$	[92]	2.00
N116	$OH + CH_2O \rightarrow H_2O + CHO$	$4.73 \times 10^{-12} (T_g/298)^{1.18} \exp(-224.9/T_g)$	[92]	10.0
N117	$HO_2 + C_2H_5O_2 \rightarrow C_2H_5OOH + O_2$	$3.80 \times 10^{-13} \exp(900.0/T_g)$	[102]	0.20
N118	$H + CH_2OH \rightarrow CH_3OH$	$2.89 \times 10^{-10} (T_g/298)^{0.040}$	[126]	2.00
N119	$O + CH_3OH \rightarrow OH + CH_2OH$	$7.11 \times 10^{-12} \exp(-1020.0/T_g)$	[127]	2.00
N120	$O_2 + CH_2OH \rightarrow CH_2O + HO_2$	$3.77 \times 10^{-15} (T_g/298)^{5.94} \exp(2280.5/T_g)$	[128]	0.25
N121	$OH + CH_3OH \rightarrow H_2O + CH_2OH$	$3.44 \times 10^{-13} (T_g/298)^{2.8} \exp(-210.5/T_g)$	[129]	0.40
N122	$OH + CH_3OH \rightarrow H_2O + CH_3O$	$1.66 \times 10^{-11} \exp(-854.0/T_g)$	[102]	3.16
N123	$OH + CH_3OH \rightarrow H_2O + CH_2O + H$	$1.10 \times 10^{-12} (T_g/298)^{1.44} \exp(-56.53/T_g)$	[130]	0.50
N124	$OH + CH_5OH \rightarrow H_2O + C_2H_5O$	$5.28 \times 10^{-11} (T_g/298)^{0.54} \exp(-50.5/T_g)$	[102]	0.08
N125	$OH + CH_5OOH \rightarrow H_2O + C_2H_5O_2$	$3.00 \times 10^{-12} \exp(190.0/T_g)$	[92]	0.30

N126	$C_2H + H \rightarrow C_2H_2$	3.01×10^{-10}	[91]	1.50
N127	$C_2H + CH_4 \rightarrow C_2H_2 + CH_3$	$3.01 \times 10^{-12} \exp(-250.2/T_g)$	[91]	3.00
N128	$C_2H + C_2H_4 \rightarrow C_2H_2 + C_2H_3$	1.40×10^{-10}	[131]	2.00

(a) The primary source was not accessible and/or the uncertainty was not given, so the uncertainty was assumed based on the dispersion of the literature data.

Reference

[1] Solomon, S.; Qin, D. ; Manning, M. ; Marquis, M. ; Averyt, K.; Tignor, M. M. B.; Miller, H. L. ; Z. Chen. Eds., Climate Change 2007: The Physical Science Basis. Contribution of Working Group I to the Fourth Assesment Report of the Intergovernmental Panel on Climate Change. New York: Cambridge University Press, 2007.

[2] Lunsford, J. H. Catalytic Conversion of Methane to More Useful Chemicals and Fuels: a Challenge for the 21st Century. *Catal. Today* **2000**, *63*,165–174.

[3] McDonough, W.; Braungart, M.; Anastas, P.; Zimmerman, J. Applying the Principles of Green Engineering to Cradle-to-Cradle Design. *Environ. Sci. Technol.* **2003**, *37*, 434A–441A.

[4] Edwards, J. H.; Maitra, A. M. The Chemistry of Methane Reforming with Carbon Dioxide and its Current and Potential Applications. *Fuel Process. Technol.***1995**, *42*, 269-289.

[5] Rostrup-Nielsen, J. R. Aspects of CO_2-reforming of Methane. *Stud. Surf. Sci. Catal.***1994**, *81*, 25-41.

[6] Bradford, M. C. J.; Vannice, M. A. CO_2 Reforming of CH_4. *Cat. Rev.***1999**, *41*, 1-42.

[7] Ross, R. H. Natural Gas Reforming and CO_2 Mitigation. *Catal.Today* **2005**, *100 (1−2)*, 151−158.

[8] Treacy, D.; Ross, J. R. H. Carbon Dioxide Reforming of Methane over Supported Molybdenum Carbide Catalysts. *Prepr. Pap.-Am. Chem. Soc., Div. Fuel Chem.* **2004**, *49 (2)*, 643−644.

[9] Snoeckx, R.; Bogaerts, A. Plasma Technology − a Novel Solution for CO_2 Conversion? *Chem. Soc. Rev.* **2017**, *46*, 5805−586.

[10] Kogelschatz, U. Dielectric-barrier Discharges: Their History, Discharge Physics, and Industrial Applications. *Plasma Chem. Plasma Process*. **2003**, *23*, 1–46.

[11] Zou, J. J. ; Zhang, Y. P. ; Liu, C. J. ; Li, Y.; Eliasson, B. Starch-enhanced Synthesis of Oxygenates from Methane and Carbon Dioxide using Dielectric-barrier Discharges. *Plasma Chem. Plasma Process.* **2003**, *23*, 69−82.

[12] Liu, C. J.; Xue, B.; Eliasson, B.; He, F.; Li, Y.; Xu, G.-H. Methane Conversion to Higher Hydrocarbons in the Presence of Carbon Dioxide Using Dielectric-Barrier Discharge Plasmas. *Plasma Chem. Plasma Process.* **2001**, *21 (3)*, 301−310.

[13] Tu, X.; Whitehead, J. C. Plasma-Catalytic Dry Reforming of Methane in an Atmospheric Dielectric Barrier Discharge: Understanding the Synergistic Effect at Low Temperature. *Appl. Catal. B: Environ.* **2012**, *125*, 439−448.

[14] Wang, L.; Yi, Y. H.; Wu, C. F.; Guo, H. C. ; Tu, X. One-step Reforming of CO_2 and CH_4 to High-value Liquid Chemicals and Fuels at Room Temperature by Plasma-driven Catalysis. *Angewandte Chemie International Edition* **2017**, *56*, 13679-13683.

[15] Zeng, Y. X. ; Wang, L. ; Wu, C. F. ; Wang, J. Q. ; Shen, B. X.; Tu, X. Low Temperature Reforming of biogas over K-, Mg- and Ce-promoted Ni/Al_2O_3 Catalysts for the Production of Hydrogen Rich Syngas: Understanding Plasma-catalytic Synergy. *Appl. Catal. B: Environ.* **2018**, *224*, 469-478.

[16] Zhang, X.; Cha, M. S. Electron-Induced Dry Reforming of Methane in a Temperature-Controlled Dielectric Barrier Discharge Reactor. *J. Phys. D. Appl. Phys.* **2013**, *46* (41), 415205.

[17] Zhang, X.; Cha, M. S. Partial Oxidation of Methane in a Temperature-Controlled Dielectric Barrier Discharge Reactor. *Proc. Combust. Inst.* **2015**, *35* (3), 3447–3454.

[18] Nair, S. A.; Nozaki, T.; Okazaki, K. Methane Oxidative Conversion Pathways in a Dielectric Barrier Discharge Reactor -Investigation of Gas Phase Mechanism. *Chem. Eng. J.* **2007**, *132 (1−3)*, 85−95.

[19] Wang, Q.; Yan, B.-H.; Yin, Y.; Cheng, Y. Investigation of Dry reforming of Methane in a Dielectric Barrier Discharge Reactor. *Plasma Chem. Plasma Process.* **2009**, *29 (3)*, 217−228.

[20] Kraus, M.; Egli, W.; Haffner, K.; Eliasson, B.; Kogelschatz, U.; Wokaun, A. Investigation of Mechanistic Aspects of the Catalytic CO_2 Reforming of Methane in a Dielectric-Barrier Discharge Using Optical Emission Spectroscopy and Kinetic Modeling. *Phys. Chem. Chem. Phys.* **2002**, *4 (4)*, 668−675.

[21] Scarduelli, G.; Guella, G.; Ascenzi, D.; Tosi, P. Synthesis of Liquid Organic Compounds from CH_4 and CO_2 in a Dielectric Barrier Discharge Operating at Atmospheric Pressure. *Plasma Process. Polym.* **2011**, *8*, 25−31.

[22] Goujard, V.; Tatiboue, J.-M.; Batiot-Dupeyrat, C. Carbon Dioxide Reforming of Methane Using a Dielectric Barrier Discharge Reactor: Effect of Helium Dilution and Kinetic Model. *Plasma Chem. Plasma Process.* **2011**, *31*, 315−325.

[23] Luche, J.; Aubry, O.; Khacef, A.; Cormier, J.-M. Syngas Production from Methane Oxidation Using a Non-Thermal Plasma: Experiments and Kinetic Modeling. *Chem. Eng. J.* **2009**, *149* (1–3), 35–41.

[24] Zhou, L. M.; Xue, B.; Kogelschatz, U.; Eliasson, B. Nonequilibrium Plasma Reforming of Greenhouse Gases to Synthesis Gas. *Energy & Fuels* **1998**, *12* (6), 1191–1199.

[25] Machrafi, H.; Cavadias, S.; Amouroux, J. Valorization by Means of Dielectric Barrier Discharge. *J. Phys. Conf. Ser.* **2011**, *275*, 12016.

[26] Goujard, V.; Tatibouët, J. M.; Batiot-Dupeyrat, C. Carbon Dioxide Reforming of Methane Using a Dielectric Barrier Discharge Reactor: Effect of Helium Dilution and Kinetic Model. *Plasma Chem. Plasma Process.* **2011**, *31* (2), 315–325.

[27] Wang, J. G.; Liu, C. J.; Eliassion, B. Density Functional Theory Study of Synthesis of Oxygenates and Higher Hydrocarbons from Methane and Carbon Dioxide Using Cold Plasmas. *Energy & Fuels* **2004**, *18* (1), 148–153.

[28] Istadi, I.; Amin, N. A. S. Modelling and Optimization of Catalytic-Dielectric Barrier Discharge Plasma Reactor for Methane and Carbon Dioxide Conversion Using Hybrid Artificial Neural Network-Genetic Algorithm Technique. *Chem. Eng. Sci.* **2007**, *62* (23), 6568–6581.

[29] Kraus, M.; Egli, W.; Haffner, K.; Eliasson, B.; Kogelschatz, U.; Wokaun, A. Investigation of Mechanistic Aspects of the Catalytic CO_2 Reforming of Methane in a Dielectric-Barrier Discharge

Using Optical Emission Spectroscopy and Kinetic Modeling. *Phys. Chem. Chem. Phys.* **2002**, *4* (4), 668–675.

[30] Liu, C.-J.; Li, Y.; Zhang, Y.-P.; Wang, Y.; Zou, J.; Eliasson, B.; Xue, B. Production of Acetic Acid Directly from Methane and Carbon Dioxide Using Dielectric-Barrier Discharges. *Chem. Lett.* **2001**, *30* (12), 1304–1305.

[31] Wang, W.; Patil, B.; Heijkers, S.; Hessel, V.; Bogaerts, A. Nitrogen Fixation by Gliding Arc Plasma: Better Insight by Chemical Kinetics Modelling. ChemSusChem **2017**, *10*, 2145–2157

[32] Wang, W.; Berthelot, A.; Kolev, S.; Tu, X.; Bogaerts, A. CO_2 Conversion in a Gliding Arc Plasma: 1D Cylindrical Discharge Model. *Plasma Sources Sci. Technol.* **2016**, *25* (6), 65012.

[33] Wang, W.; Mei, D.; Tu, X.; Bogaerts, A. Gliding Arc Plasma for CO_2 Conversion: Better Insights By a Combined Experimental and Modelling Approach. *Chem. Eng. J.* **2017**, *330*, 11-25.

[34] Wang, W.; Snoeckx, R.; Zhang, X. M.; Cha, M. S.; Bogaerts, A. Modeling Plasma-based CO_2 and CH_4 Conversion in Mixtures with N_2, O_2, and H_2O: The Bigger Plasma Chemistry Picture. *J. Phys. Chem. C* **2018**, DOI: 10.1021/acs.jpcc.7b10619.

[35] Janeco, A.; Pinha, N. R.; Guerra, V. Electron Kinetics in He / CH_4 / CO_2 Mixtures Used for Methane Conversion. *J. Phys. Chem. C* **2015**, *119*, 109.

[36] Snoeckx, R.; Aerts, R.; Tu, X.; Bogaerts, A. Plasma-Based Dry Reforming: A Computational Study Ranging from the Nanoseconds to Seconds Time Scale. *J. Phys. Chem. C* **2013**, *117* (10), 4957–4970.

[37] Snoeckx, R.; Zeng, Y. X.; Tu, X.; Bogaerts, A. Plasma-Based Dry Reforming: Improving the Conversion and Energy Efficiency in a Dielectric Barrier Discharge. *RSC Adv.* **2015**, *5* (38), 29799–29808.

[38] De Bie, C.; Martens, T.; van Dijk, J.; Paulussen, S.; Verheyde, B.; Corthals, S.; Bogaerts, A. Dielectric Barrier Discharges Used for the Conversion of Greenhouse Gases: Modeling the Plasma Chemistry by Fluid Simulations. *Plasma Sources Sci. Technol.* **2011**, *20* (2), 24008.

[39] De Bie, C.; Van Dijk, J.; Bogaerts, A. The Dominant Pathways for the Conversion of Methane into Oxygenates and Syngas in an Atmospheric Pressure Dielectric Barrier Discharge. *J. Phys. Chem. C* **2015**, *119* (39), 22331–22350.

[40] Bogaerts, A.; Wang, W. Z.; Berthelot A.; Guerra, V. Modeling Plasma-based CO_2 Conversion: Crucial Role of the Dissociation Cross Section. *Plasma Sources Sci. Technol.* **2016**, *25*, 055016.

[41] Turner, M. M. Uncertainty and Error in Complex Plasma Chemistry Models. *Plasma Sources Sci. Technol.* **2015**, *24*, 035027.

[42] Turner, M. M. Uncertainty and Sensitivity Analysis in Complex Plasma Chemistry Models. *Plasma Sources Sci. Technol.* **2016**, *25*, 015003.

[43] Turner, M. M. Computer Simulation in Low-Temperature Plasma Physics: Future Challenges. *Plasma Process. Polym.* **2017**, *14*, 1600121.

[44] Berthelot, A.; Bogaerts, A. Modeling of CO_2 Plasma: Effect of Uncertainties in the Plasma Chemistry. *Plasma Sources Sci. Technol.* **2017**, *26*, 115002.

[45] Pancheshnyi, S.; Eismann, B. ; Hagelaar G. J. M. ; Pitchford, L. C. Computer code ZDPlasKin, University of Toulouse, LAPLACE, CNRS-UPS-INP, Toulouse, France, 2008, http://www.zdplaskin.laplace.univ-tlse.fr.

[46] Aerts, R.; Somers, W.; Bogaerts, A. Carbon Dioxide Splitting in a Dielectric Barrier Discharge Plasma: A Combined Experimental and Computational Study. *ChemSusChem* **2015**, *8 (4)*, 702–716.

[47] Hagelaar, G. J. M.; Pitchford, L. C. Solving the Boltzmann equation to obtain electron transport coefficients and rate coefficients for fluid models. *Plasma Sources Sci.Technol*. **2005**, *14*, 722–733.

[48] M. Alvo and P. L. Yu, Statistical Methods for Ranking Data. No. 1976, New York, NY: Springer New York, 2014.

[49] Fridman, A. Plasma Chemistry; Cambridge University Press: New York, 2008.

[50] Aerts, R.; Martens T.; Bogaerts, A. Influence of Vibrational States on CO_2 Splitting by Dielectric Barrier Discharges. *J. Phys. Chem. C* **2012**, *116*, 23257.

[51] Itikawa, Y. Cross Sections for Electron Collisions with Carbon Dioxide. *J. Phys. Chem. Ref. Data* **2002**, *31*, 749–767.

[52] Lowke, J. J. ; Phelps A. V.; Irwin, B. W. Predicted Electron Transport Coefficients and Operating Characteristics of CO_2–N_2–He Laser Mixtures. *J. Appl. Phys.* **1973**, *44*, 4664–4671.

[53] Hake R. D. Jr.; Phelps, A. V. Momentum-transfer and Inelastic-collision Cross Sections for Electrons in O_2, CO, and CO_2. *Phys. Rev.* **1967**, *158*, 70–84.

[54] Polak L. S.; Slovetsky, D. I. Electron Impact Induced Electronic Excitation and Molecular Dissociation. *Int. J. Radiat. Phys. Chem.* **1976**, *8*, 257–282.

[55] Land, J. E. Electron Scattering Cross Sections for Momentum Transfer and Inelastic Excitation in Carbon Monoxide. *J. Appl. Phys.* **1978**, *49*, 5716–5721.

[56] Mangan, M. A. ; Lindsay B. G. ; Stebbings, R. F. Absolute Partial Cross Sections for Electron-Impact Ionization of CO from Threshold to 1000 eV. *J. Phys. B: At. Mol. Opt. Phys.* **2000**, *33*, 3225-3234.

[57] Lawton S. A. ; Phelps, A. V. Total and Partial Ionization Cross Sections of Atoms and Ions by Electron Impact Atom. *J. Chem. Phys.* **1978**, *69*, 1055–1068.

[58] W. L. Morgan, Kinema Research & Software, LXcat database.

[59] Janev, R. K.; Murakami, I. ; Kato T.; Wang, J. Cross Sections and Rate Coefficients for Electron-Impact Ionization of Hydrocarbon Molecules. Toki, Gifu, Japan, 2001.

[60] Janev R. K.; Reiter, D. Collision Processes of CH_y and CH_y^+ Hydrocarbons with Plasma Electrons And Protons. *Phys. Plasmas* **2002**, *9*, 4071–4081.

[61] Janev, R. K. Collision Processes of Hydrocarbon Species in Hydrogen Plasmas. Part 1. The Methane Family. *ChemInform* **2003**, *34*, 1–47.

[62] Janev, R. K.; Murakami, I. ; Kato T.; Wang, J. Cross Sections and Rate Coefficients for Electron-Impact Ionization of Hydrocarbon Molecules. Toki, Gifu, Japan, 2001.

[63] Janev R. K.; Reiter, D. Collision Processes of Hydrocarbon Species in Hydrogen Plasmas. Part 2. The Ethane and Propane Families. *ChemInform* **2003**, *34*, 1–124.

[64] Janev R. K.; Reiter, D. Collision Processes of $C_{2,3}H_y$ and $C_{2,3}H_y^+$ Hydrocarbons with Electrons and Proton. *Phys. Plasmas* **2004**, *11*, 780–829.

[65] Phelps Database, www.lxcat.net. Buckman S. J. ; Phelps, A. V. JILA Information Center Report No. 27, University of Colorado (May 1, 1985), Vibrational Excitation of D_2 by Low Energy Electrons. *J. Chem. Phys.***1985**, *82*, 4999.

[66] IST-Lisbon database, www.lxcat.net. Marques, L.; Jolly, J. ; Alves, L. L. Capacitively Coupled Radio-Frequency Hydrogen Discharges: The Role of Kinetics. *J. Appl. Phys.* **2007**, *102*, 063305.

[67] Levko D. Hydrogen Kinetics in Non-Equilibrium Plasma in the Electrical Discharge in $Ar/CH_3OH/H_2O$ Mixture. Eprint arXiv:1007.3449; 2010.

[68] Itikawa Y.; Mason, N. Cross sections for Electron Collisions with Water Molecules. *J. Phys. Chem. Ref. Data* **2005**, *34*, 1–22.

[69] Janev, R. K. ; Reiter D. ; Samm, U. Collision Processes in Low-temperature Hydrogen Plasmas 2003, Technical Report Forschungszentrum Juelich GmbH.

[70] Pedersen, H. ; Djuri´c, N. ; Jensen, M. ; Kella, D.; Safvan, C. ; Schmidt, H. ; Vejby-Christensen L. ; Andersen, L. *Phys. Rev. A* **1999**, *60*, 2882–2899.

[71] Riahi, R. ; Teulet, P. ; Ben Lakhdar Z. ; Gleizes, A. Cross-section and Rate Coefficient Calculation for Electron Impact Excitation, Ionisation and Dissociation of H_2 and OH Molecules. *Eur. Phys. J. D* **2006**, *40*, 223–230.

[72] Eliasson, B. ; Hirth M.; Kogelschatz, U. Ozone Synthesis from Oxygen in Dielectric Barrier Discharges. *J. Phys. D. Appl. Phys.* **1987**, *20*, 1421–1437.

[73] Weller, C. S. and Biondi M. A. Measurements of dissociative Recombination of CO_2^+ Ions with Electrons. *Phys. Rev. Lett.* **1967**,*19*, 59–61

[74] Thoenes, J. and Kurzius, S. C. 1979 Plasma chemistry processes in the closed cycle EDL Technical Report DRCPM-HELCR- 79-11-VOL-1 Lockheed Missiles and Space Co Inc. Huntsville, AL.

[75] Beuthe, T. G. and Chang, J-S. Chemical Kinetic Modelling of Non-equilibrium Ar-CO_2 thermal Plasmas. *Japan. J. Appl. Phys.* **1997**, *36*, 4997–5002.

[76] Mcelroy, D.; Walsh, C.; Markwick, A. J.; Cordiner, M. A.; Smith, K. and Millar, T. J. The UMIST Database for Astrochemistry 2012. *Astron. Astrophys*. **2013**, *550*, A36.

[77] Mitchell, J. B. A. and Hus, H. The Dissociative Recombination and Excitation of CO^+. *J. Phys. B: At. Mol. Phys.* **1985**, *18*, 547–555.

[78] Cenian, A.; Chernukho A.; Borodin, V. Modeling of Plasma-chemical Reactions in Gas Mixture of CO_2 Lasers. II. Theoretical Model and its Verification. *Contrib. Plasma Phys.* **1995**, *35*, 273-296.

[79] Florescu-Mitchell, A. I.; Mitchell, J. B. A. Dissociative Recombination. *Phys. Rep.* **2006**, *430*, 277-374.

[80] Woodall, J.; Ag´undez, M.; Markwick-Kemper A. J.; Millar, T. J. The UMIST Database for Astrochemistry 2006. *Astronom. Astrophys.* **2007**, *466*, 1197–1204.

[81] Van Gaens W. ; Bogaerts, A. Kinetic Modelling for an Atmospheric Pressure Argon Plasma Jet in Humid Air. *J. Phys. D. Appl. Phys.* **2013**, *46*, 275201.

[82] Albritton D. Ion-neutral Reaction-rate Constants Measured in Flow Reactors through 1977. *At. Data Nucl. Data Tables* **1978**, *22*, 1–101

[83] Adams, N.; Smith, D.; Grief, D. Reactions of H_nCO^+ ions with molecules at 300 K. *Int. J. Mass Spectrom. Ion Phys.* **1978**, *26*, 405–415

[84] Hokazono, H.; Fujimoto, H. Theoretical Analysis of the CO_2 Molecule Decomposition and Contaminants Yield in Transversely Excited Atmospheric CO_2 Laser Discharge. *J. Appl. Phys.* **1987**, *62*, 1585.

[85] Price, D.; Moruzzi, J. Negative Ion Molecule Reactions in CO_2 at High Pressures and Temperatures. *Vacuum* **1974**, *24*, 591–3

[86] Fehsenfeld, F. C.; Schmeltekopf, A. L.; Schiff, H. I.; Ferguson, E. E. Laboratory Measurements of Negative Ion Reactions of Atmospheric Interest Planet. *Space Sci.* **1967**, *15* 373–379.

[87] Kim, Y. H.; Fox, J. L. The Chemistry of Hydrocarbon Ions in the Jovian Ionosphere. *Icarus* **1994**, *112*, 310-325.

[88] Tahara, H.; Minami, K.; Murai, A.; Yasui, T.; Yoshikawa, T. Diagnostic Experiment and Kinetic-model Analysis of Microwave CH_4/H_2 Plasmas for Deposition of Diamond-Like Carbon-films. *Jpn. J. Appl. Phys.* **1995**, *34*, 1972-1979.

[89] Eliasson, B. ; Hirth M.; Kogelschatz, U. Ozone Synthesis from Oxygen in Dielectric Barrier Discharges. *J. Phys. D. Appl. Phys.* **1987**, *20*, 1421–1437.

[90] Kossyi, I. A. ; Kostinsky, A. Y. ; Matveyev A. A.; Silakov, V. P. Kinetic Scheme of the Non-Equilibrium Discharge in Nitrogen-Oxygen Mixtures. *Plasma Sources Sci. Technol.* **1992**, *1*, 207–220.

[91] Tsang, W.; Hampson, R. F. Chemical Kinetic Data Base for Combustion Chemistry. Part I. Methane and Related Compounds. *J. Phys. Chem. Ref. Data* **1986**, *15*, 1087-1279.

[92] Baulch, D. L.; Cobos, C. J.; Cox, R. A. ; Esser, C.; Frank, P. ; Just, T. ; Kerr, J. A. ; Pilling, M. J.; Troe, J. ; Walker R. W. ; Warnat, J. Evaluated Kinetic Data for Combustion Modelling. *J. Phys. Chem. Ref. Data* **1992**, *21*, 411-734.

[93] Lin, S. Y.; Guo, H. Case study of a Prototypical Elementary Insertion Reaction: $C(^1D)+H_2$ -> CH+H. *J. Phys. Chem. A* **2004**, *108*, 10066-10071.

[94] Tsang, W. Chemical Kinetic Data Base for Combustion Chemistry. Part 3: Propane. *J. Phys. Chem. Ref. Data* **1988**, *17*, 887-951.

[95] Kurylo, M. J. ; Peterson, N. C. ; Braun, W. Absolute Rates of the Reactions H + C_2H_4 and H + C_2H_5, *J. Chem. Phys.* **1970**, *53*, 2776.

[96] Harding, L. B.; Georgievskii, Y.; Klippenstein, S. J. Predictive Theory for Hydrogen Atom - Hydrocarbon Radical Association Kinetics. *J. Phys. Chem. A* **2005**, *109*, 4646-4656.

[97] Halberstadt, M. L.; Crump, J. Insertion of Methylene into the Carbon-Hydrogen Bonds of the C1 to C4 Alkanes. *J. Photochem.* **1973**, *1*, 295-395.

[98] Baulch, D. L.; Bowman, C. T.; Cobos, C. J. ; Cox, R. A. ; Just, T. ; Kerr, J. A.; Pilling, M. J. ; Stocker, D.; Troe, J. ; Tsang, W. et al. Evaluated Kinetic Data for Combustion Modeling: Supplement II. *J. Phys. Chem. Ref. Data* **2005**, *34*, 757-1397.

[99] Atkinson, R.; Baulch, D. L. ; Cox, R. A. ; Hampson, R. F. ; Kerr, J. A. ; Troe, J. Evaluated Kinetic and Photochemical Data for Atmospheric Chemistry. 3. Iupac Subcommittee on Gas Kinetic Data Evaluation for Atmospheric Chemistry. *J. Phys. Chem. Ref. Data* **1989**, *18*, 881- 1097.

[100] Warnatz, J. Rate Coefficients in the C/H/O System, 1984, Combustion Chemistry ed. Gardiner, W. C., Jr., Springer-Verlag, NY.

[101] Sun, H.; Tang, Y. Z. ; Wang, Z. L. ; Pan, X. M. ; Li, Z. S. ; Wang, R. S. DFT Investigation of the Mechanism of CH_2CO+O(P-3) Reaction. *Int. J. Quantum Chem.* **2005**, *105*, 527-532.

[102] Atkinson, R.; Baulch, D. L.; Cox, R. A.; Crowley, J. N.; Hampson, R. F. ; Hynes, R. G. ; Jenkin, M. E.; Rossi, M. J.; Troe, J. Evaluated kinetic and Photochemical Data for Atmospheric Chemistry: Volume II - Gas Phase Reactions of Organic Species. *Atmos. Chem. Phys.* **2006**, *6*, 3625-4055.

[103] Tsang, W. Chemical Kinetic Data Base for Combustion Chemistry. Part 2. Methanol. *J. Phys. Chem. Ref. Data* **1987**, *16*, 471-508.

[104] Heidner III, R. F.; Husain, D. Electronically Excited Oxygen Atoms O (21D2). A Time-resolved Study of the Collisional Quenching by the Gases H_2, D_2, NO, N_2O, CH_4, and C_3O_2 using Atomic Absorption Spectroscopy in the Vacuum Ultraviolet. *Int. J. Chem. Kinet.* **1973**, *5*, 819–831.

[105] Bradley, J. N.; Edwards, A. D.; Gilbert, J. R. The Gas-phase Reactions of Singlet Oxygen Atoms with Methane. *J. Chem. Soc. A* **1971**, 326 – 331.

[106] Atkinson, R.; Baulch, D.L.; Cox, R.A.; Hampson, R.F., Jr.; Kerr, J.A.; Rossi, M.J.; Troe, J. Evaluated Kinetic, Photochemical and Heterogeneous Data for Atmospheric Chemistry: Supplement V, IUPAC Subcommittee on Gas Kinetic Data Evaluation for Atmospheric Chemistry. *J. Phys. Chem. Ref. Data* **1997**, *26*, 521 – 1011.

[107] Chang, A.H H.; Lin, S.H. A theoretical study of the O(1D)+CH_4 reaction II. *Chem. Phys. Lett.* **2004**, *384*, 229 – 235.

[108] Tully, J. C. Reactions of O(1D) with Atmospheric Molecules. *J. Chem. Phys.***1975**, *62*, 1893.

[109] Noxon, J. F. Optical Emission from O(1D) And O_2(B1ΣG) in Ultraviolet Photolysis of O_2 and CO_2. *J. Chem. Phys.* **1970**, *52*, 1852 – 1873.

[110] Dean, A. M.; Kistiakowsky, G. B. Oxidation of Carbon Monoxide/Methane Mixtures in Shock Waves. *J. Chem. Phys.* **1970**, *54*, 1718 – 1725.

[111] Capitelli, M.; Ferreira, C. M. ; Gordiets B. F. ; Osipov, A. I. Plasma Kinetics in Atmospheric Gases (2000) Springer.

[112] Atkinson, R. ; Baulch, D. L. ; Cox, R. A.; Hampson, Jr. R. F. ; Kerr, J. A. ; Troe, J. Evaluated Kinetic and Photochemical Data for Atmospheric Chemistry. Supplement IV, IUPAC Subcommittee on Gas Kinetic Data Evaluation for Atmospheric Chemistry. *J. Phys. Chem. Ref. Data* **1992**, *21*, 1125 – 156.

[113] Bauerle, S.; Klatt, M.; Wagner, H.Gg. Recombination and Decomposition of Methylene Radicals at High Temperatures. *Ber. Bunsenges. Phys. Chem.***1995**, *99*, 870 – 879.

[114] Pintassilgo, C. D.; Jaoul, C.; Loureiro, J.; Belmonte, T.; Czerwiec, T. Kinetic Modelling of a N_2 Flowing Microwave Discharge with CH_4 Addition in the Post-Discharge for Nitrocarburizing Treatments. *J. Phys. D. Appl. Phys.* **2007**, *40* (12), 3620–3632

[115] Harding, R. Guadagnini, G. C. Schatz. Theoretical-studies of the Reactions H+CH->C+H_2 and C+H_2->CH_2 using an Abinitio Global Ground-State Potential Surface for CH_2. *J. Phys. Chem.* **1993**, *97*, 5472-5481.

[116] Baulch, D. L.; Cobos, C. J. ; Cox, R. A.; Frank, P. ; Hayman, G. ; Just, T. ; Kerr, J. A. ; Murrells, T. ; Pilling, M. J. ; Troe, J. et al. Evaluated Kinetic Data for Combustion Modeling - Supplement-1. *J. Phys. Chem. Ref. Data* **1994**, *23*, 847-1033.

[117] Harding, L. B.; Georgievskii, Y.; Klippenstein, S. J. Predictive Theory for Hydrogen Atom - Hydrocarbon Radical Association Kinetics. *J. Phys. Chem. A* **2005**, *109*, 4646-4656.

[118] Hadj-Ziane , S.; Held, B.; Pignolet, P.; Peyrous, R.; Coste, C. Ozone Generation in an Oxygen-Fed Wire-To- Cylinder Ozonizer at Atmospheric Pressure. *J. Phys. D: Appl. Phys.* **1992**, *25*, 677.

[119] Bonard, A.; Daele, V.; Delfau, J.-L.; Vovelle, C. Kinetics of OH Radical Reactions with Methane in the Temperature Range 295-660 K and with Dimethyl Ether and Methyl-Tert-Butyl Ether in the Temperature Range 295-618 K. *J. Phys. Chem. A* **2002**, *106*, 4384-4389.

[120] Humpfer, R.; Oser, H.; Grotheer, H-H.; Just, T. The Reaction System CH_3 + OH at Intermediate Temperatures. Appearance of a New Product Channel. *Symp. Int. Combust. Proc.* **1994**, *25*, 721-731.

[121] Lloyd, A. C. Evaluated and Estimated Kinetic Data for Phase Reactions of the Hydroperoxyl Radical. *Int. J. Chem. Kinet.* **1974**, *6*, 169-228.

[122] Atkinson, R.; Baulch, D. L. ; Cox, R. A. ; Crowley, J. N. ; Hampson, R. F. ; Hynes, R. G.; Jenkin, M. E. ; Rossi, M. J. ; Troe, J. Evaluated Kinetic and Photochemical Data for Atmospheric Chemistry: Volume I - Gas Phase Reactions of O_x, HO_x, NO_x And SO_x Species. *Atmos. Chem. Phys.* **2004**, *4*, 1461-1738.

[123] Miller, J. A.; Garrett, B. C. Quantifying the Non-RRKM Effect in the H + O_2 = OH + O Reaction. *Int. J. Chem. Kinet.* **1997**, *29*, 275-287.

[124] Shaw, R. Estimation of Rate Constants as a Function of Temperature for the Reactions W + XYZ = WX + YZ, where W, X, Y, and Z are H or O Atoms. *Int. J. Chem. Kinet.* **1977**, *9*, 929-941.

[125] Cobos, C. J.; Troe, J. Theory of Thermal Unimolecular Reactions at High Pressures. II. Analysis of Experimental Results. *J. Chem. Phys.* **1985**, *83*, 1010-1015.

[126] Delbos, E. ; Fittschen, C. ; Hippler, H. ; Krasteva, N. ; Olzmann, M.; Viskolcz, B. Rate Coefficients and Equilibrium Constant for the CH_2CHO+O_2 Reaction System. *J. Phys. Chem. A* **2006**, *110*, 3238-3245.

[127] Basevich, V.Ya.; Kogarko, S.M.; Furman, G. A.The Reactions of Methanol with Atomic Oxygen. B*ull. Acad. Sci. USSR Div. Chem. Sci.* (Engl. Transl.) **1975**, *24*, 948-952.

[128] Grotheer, H.; Riekert, G.; Walter, D. Th. Just, Non-arrhenius Behavior of the Reaction of Hydroxymethyl Radicals with Molecular Oxygen. *J. Phys. Chem.* **1988**, *92*, 4028-4030.

[129] Jodkowski, J. T.; Rayez, M. T.; Rayez, J. C.; Berces, T. ; Dobe, S. Theoretical Study of the Kinetics of the Hydrogen Abstraction from Methanol. 3. Reaction of Methanol with Hydrogen Atom, Methyl, and Hydroxyl Radicals. *J. Phys. Chem. A* **1999**, *103*, 3750-3765.

[130] Srinivasan, N. K. ; Su, M. C. ; Michael, J. V. High-temperature Rate Constants for CH_3OH+Kr -> Products, OH+CH_3OH -> Products, OH+$(CH_3)CO$ -> CH_2COCH_3+H_2O, and OH+CH_3 -> CH_2+H_2O. *J. Phys. Chem. A* **2007**, *111*, 3951-3958.

[131] Laufer, A. H.; Fahr, A. Reactions and Kinetics of Unsaturated C_2 Hydrocarbon Radicals. *Chem. Rev.* **2004**, *104*, 2813-2832.